ISSN 0024-4902, Lithology and Mineral Resources, 2015, Vol. 50, No. 6, pp. 452–477. © Pleiades Publishing, Inc., 2015.
Original Russian Text © T.A. Ivanovskaya, B.B. Zviagina, B.A. Sakharov, T.S. Zaitseva, E.V. Pokrovskaya, O.V. Dorzhieva, 2015, published in Litologiya i Poleznye Iskopaemye, 2015, No. 6, pp. 510–537.

Globular Layer Silicates of the Glauconite–Illite Composition in Upper Proterozoic and Lower Cambrian Rocks

T. A. Ivanovskaya[a], B. B. Zviagina[a], B. A. Sakharov[a], T. S. Zaitseva[b], E. V. Pokrovskaya[a], and O. V. Dorzhieva[c]

[a]*Geological Institute, Russian Academy of Sciences, Pyzhevskii per. 7, Moscow, 119017 Russia*
e-mail: tat.ivanovskaya2012@yandex.ru; zbella2001@yahoo.com
[b]*Institute of Precambrian Geology and Geochronology, Russian Academy of Sciences, nab. Makarova 2, St. Petersburg, 199034 Russia*
[c]*Institute of Geology of Ore Deposits, Petrography, Mineralogy, and Geochemistry, Russian Academy of Sciences, Staromonetnyi per. 35, Moscow, 119017 Russia*

Received December 29, 2014

Abstract—The paper presents the generalized results of structural and crystal-chemical study of globular dioctahedral 2 : 1 layer silicates of the glauconite–illite composition (45 samples) taken from the Lower Cambrian sequences of North Siberia (Olenek Uplift); Riphean, Vendian, and Lower Cambrian sequences of East Siberia; Upper Riphean sequences of the South Urals and Srednii Peninsula; and Vendian–Cambrian boundary rocks of the Podolian Dniester region (Ukraine). Monomineral fractions of grains were studied using modern chemical and physical methods: X-ray analysis, oblique-texture electron diffraction (OTED), scanning electron microscopy (SEM), classical chemical and microprobe analyses, IR and Mössbauer spectroscopy, and others. Simulation of the experimental diffraction patterns of glycolated specimens (Sakharov et al., 1999) allowed us to determine the degree of expandability (4–13%), type of expandable layers (16.85 Å, smectite and 13.2 Å, vermiculite), their proportions in two- and three-component mixed-layers, unit cell parameters b (9.02–9.11 Å) and $c\sin\beta$ (9.94–10 Å) of mica layers, as well as the degree of short-range order in the alternation of layers of different types (R = 0, 2, 3). The classification of low-charge (layer charge ≈ 0.6–0.85 per f.u.) dioctahedral 2 : 1 layer silicates is given with account taken of the recommendations of the International Nomenclature Committee on Micas and Clay Minerals (IMA NC, AIPEA NC) (Reider et al., 1998; Guggenheim et al., 2006). Based on the crystal-chemical data on 79 samples obtained in (Ivanovskaya et al., 2012) and in the present paper, it is shown that the globular micaceous varieties are represented by a continuous isomorphic series ranging from illites through Fe-illite and Al-glauconite to glauconites ($^{VI}Al/(^{VI}Fe^{3+} + {}^{VI}Al)$ = 0.81–0.91, 0.60–0.78, 0.51–0.59, and 0.11–0.50, respectively). Following (Kossovskaya and Drits, 1971; Drits et al., 2013), we distinguish Fe-illites ($^{VI}Al/(^{VI}Fe^{3+} + {}^{VI}Al) = 0.6–0.8$) and retain the term Al-glauconite for mineral varieties with the Al index $K_{Al} = {}^{VI}Al/(^{VI}Fe^{3+} + {}^{VI}Al)$ between 0.51 and 0.59. The structural characteristics (unit cell parameters b, $c\sin\beta$, and others) and IR spectroscopic data on illite, Fe-illite, Al-glauconite, and glauconite are compared. Special attention is given to samples with elevated Mg contents found in these groups of mineral varieties. Since compositional variations of the studied glauconite–illite minerals fall beyond the fields accepted for these minerals by IMA NC and AIPEA NC, the existing classifications for low-charge dioctahedral micaceous micas may need to be revised.

DOI: 10.1134/S002449021506005X

INTRODUCTION

Up to now, problems of the classification and nomenclature of low-charge dioctahedral 2 : 1 layer silicates of the glauconite–illite composition remain debatable. According to the resolutions of the international nomenclature committees on micas (IMA NC and AIPEA NC), these silicates are subdivided into the glauconite and illite isomorphic series. They differ in Al index $K_{Al} = {}^{VI}Al/(^{VI}Fe^{3+} + {}^{VI}Al)$, which is ≤0.5 and ≥0.6, respectively, as well as in $R^{2+}/(R^{2+} + R^{3+})$ amounting for 0.15–0.42 and ≤0.25, respectively (Rieder et al., 1998; Guggenheim et al., 2006). Idealized formulas of illite and glauconite reported by IMA NC can be written as follows:

$$K_{0.8}R^{3+}_{1.33}R^{2+}_{0.67}Al_{0.13}Si_{3.87}O_{10}(OH)_2,$$

$$K_{0.65}Al_{2.0}Al_{0.65}Si_{3.35}O_{10}(OH)_2.$$

According to the recommendations of international nomenclature committees on clay minerals, the structure of true glauconites and illites are virtually devoid of expandable interlayers. If the latters are present, the samples should be classified as the mixed-layer minerals (Bailey et al., 1979, 1984). According to AIPEA NC recommendations, the term “hydromica”

is no longer used for their description (Guggenheim et al., 2006).

The low-charge (layer charge ≈ 0.6–0.85 f.u.) dioctahedral 2 : 1 layer silicates of the glauconite–illite composition were previously classified on the basis of the Fe index ($K_{Fe} = {}^{VI}Fe^{3+}/({}^{VI}Fe^{3+} + {}^{VI}Al)$) proposed in (Kossovskaya and Drits, 1971; Drits and Kossovskaya, 1991; Tsipursky and Ivanovskaya, 1988). At present, we follow the IMA NC and AIPEA NC recommendations. However, the crystal-chemical study of mica varieties showed that their cation compositions frequently do not fit the nomenclature committees' classification. In particular, the analysis of crystal-chemical peculiarities of a large collection of globular phyllosilicates of glauconit-illite composition from the Upper Proterozoic sequences of North Siberia (Anabar and Olenek uplifts) showed that they define a continuous isomorphic series (Ivanovskaya et al., 2012). The intermediate varieties of this series (K_{Al} = 0.51–0.59), which do not fit the INC classification, were ascribed to Al-glauconite or Fe-illite in compliance with the previous classification (Kossovskaya and Drits, 1971; Drits and Kossovskaya, 1991; Tsipursky and Ivanovskaya, 1988; Ivanovskaya et al., 1989). It was also noted that the IMA NC proposal to replace term "skolite" sometimes applied to designate the Al analogue of glauconite by "glauconite" proposed by (Rieder et al., 1998) is incorrect. It was also proposed that illites composing globules or large plates should be distinguished as "globular" or "platy," because green globules are traditionally called "glauconite," while the fine-dispersed Al-bearing clay minerals are called "illite" (Ivanovskaya et al., 2012).

This paper presents the generalized mineralogical characteristics of one more representative collection of globular silicates from the Lower Cambrian sequences of North Siberia (Olenek Uplift); Riphean, Vendian, and Lower Cambrian sequences of East Siberia; Upper Riphean sequence of the South Urals and Srednii Peninsula; and Vendian–Cambrian boundary rocks from the Podolian Dniester region (Ukraine). The structural and crystal-chemical features of these silicates have been published in (Ivanovskaya and Tsipursky, 1982; Ivanovskaya et al., 1985, 1989, 2003; Tsipursky et al., 1992; Ivanovskaya, 1996; Zaitseva et al., 2008), except for mineralogical characteristics of glauconite from the Lower Cambrian sequence of North Siberia (Olenek Uplift) considered here for the first time. It should be noted that the unit cell parameters *b* have been determined with high accuracy for most samples. In addition, the contents of expandable layers, $c\sin\beta$ parameters of mica layers, and short-range order factors characterizing the alternation of layers of different types in a mixed-layer structure were determined for many samples by modeling the experimental diffraction patterns of glycolated specimens (Sakharov et al., 1999).

It should also be reminded that we traditionally use the term "glauconite" to describe in general green globules varying in composition from glauconite to illite. Correspondingly, the term "glauconite" is retained for rocks containing over 50% of glauconite grains (sample 40/7, Bsh13). Their composition, in particular, is represented by Al-glauconite and Fe-illite (K_{Al} = 0.57 and 0.75).

STUDIED OBJECTS

The studied samples were taken from the Lower Cambrian sequence of North Siberia (Olenek Uplift), Vendian–Cambrian boundary rocks of the Podolian Dniester region, Upper Riphean sequences of the South Urals, upper Proterozoic sequence of East Siberia (Uchur–Maya region), and Upper Riphean rocks of the Srednii Peninsula. Locations of the studied sequences on the schematic maps of Russia and Ukraine are shown in Fig. 1a. The largest number of glauconite samples was taken from rocks of the South Urals and East Siberia. Their positions are shown in the sketch maps (Figs. 1b, 1c), while the stratigraphic assignment is demonstrated in the Riphean, Vendian, and Lower Cambrian schematic sections of the Uchur–Maya region and in the Upper Riphean section of the South Urals (Figs. 2a, 2b).

North Siberia (Olenek Uplift)

The carbonate–terrigenous Kessyusa Formation (or Group) consists of three subformations (or formations). It lies with a hiatus on dolomites of the Turkut Formation (Khorbusuonka Group) and is overlain with slight (?) erosion by the red-colored clayey limestones of the Erkeket Formation. In the Olenek and Khorbusuonka river basins, the lower subformation is represented by alternating sandstones, gravelstones, conglomerates, mudstones, sandy dolomites, and limestones (up to 30 m thick). The middle subformation is made up of alternating thin-bedded micaceous siltstones, mudstones, and silty sandstones, while its upper part contains lenses of carbonates and flat-pebble conglomerates (this subformation is up to 60 m thick). The upper subformation is made up of a wide range of rocks: limestones (including oncolitic varieties), as well as calcareous siltstones and sandstones intercalated with gravelstones, conglomerates, and mudstones (20–35 m thick). Total thickness of the formation in the Olenek and Khorbusuonka rivers is 100–125 m. Based on paleontological data, most researchers ascribe two lower subformations to the Upper Vendian, while the upper subformation of the Kessyusa Formation and the Erkeket Formation are ascribed to the Lower Cambrian (Missarzhevskii, 1980; Karlova and Vodanyuk, 1985; Vodanyuk and Karlova, 1988; Semikhatov, 2008; and others).

Separate interbeds of the Kessyusa subformations and the base of the Erkeket Formation contain glauconite with different degrees of preservation, including the fine-dispersed varieties. We only managed to

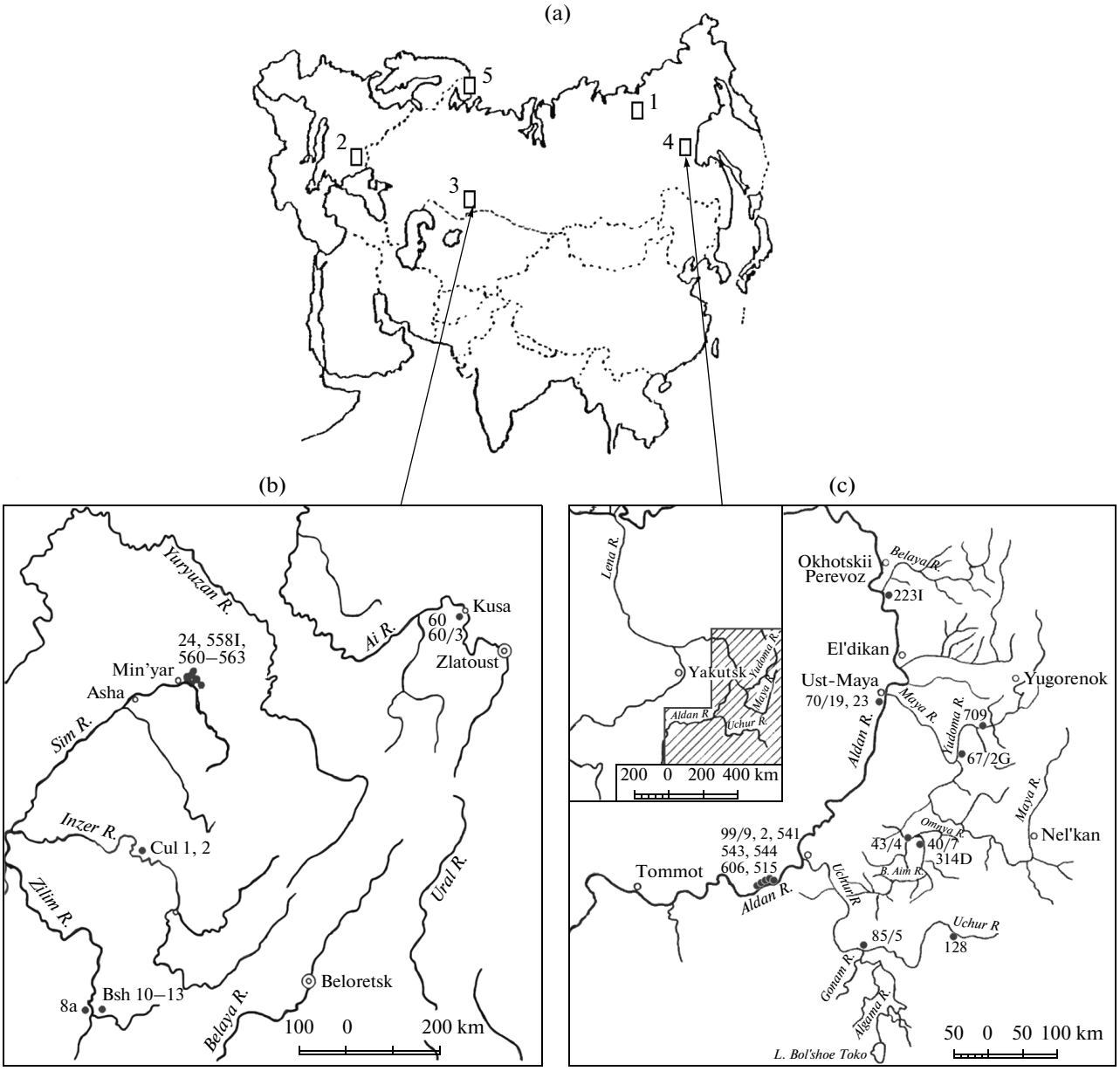

Fig. 1. Geographic position of the studied sections. (a) Section localities in the schematic map of Russian and Ukraine. (1) North Siberia (2) Podolian Dniester region, (3) South Urals, (4) East Siberia, (5) Murmansk coast, Srednii Peninsula. (b, c) Sampling locality: (b) South Urals, (c) East Siberia.

extract sufficient quantities of material for further studies from two limestone samples (samples 607 and 1783). Light gray limestones from the upper subformation of the Kessyusa Formation were taken on the right bank of the Olenek River, in front of the Suordakh River mouth, 4 m below the boundary with the Erkeket Formation. In addition, we studied sample 1783 taken from the variegated limestones at the base of the Erkeket Formation (upper reaches of the Khary-Yalakh River, right tributary of the Kyutingde River, basin of the Olenek River) kindly given to T.A. Ivanovskaya by geologists A.G. Kats and Z.B. Frolova, Cosmoaerogeological Expedition no. 3.

The Podolian Dniester Region

In the Podolian area, globular layer silicates were taken from rocks of the Khmel'nitsk Formation (55–70 m thick) ascribed to the Upper Vendian–Lower Cambrian boundary sequences. Together with the underlying Okunets and the overlying Zbruch formations, this formation belongs to the Baltic Group (*Vend Podolii*, 1990). The most complete sections of

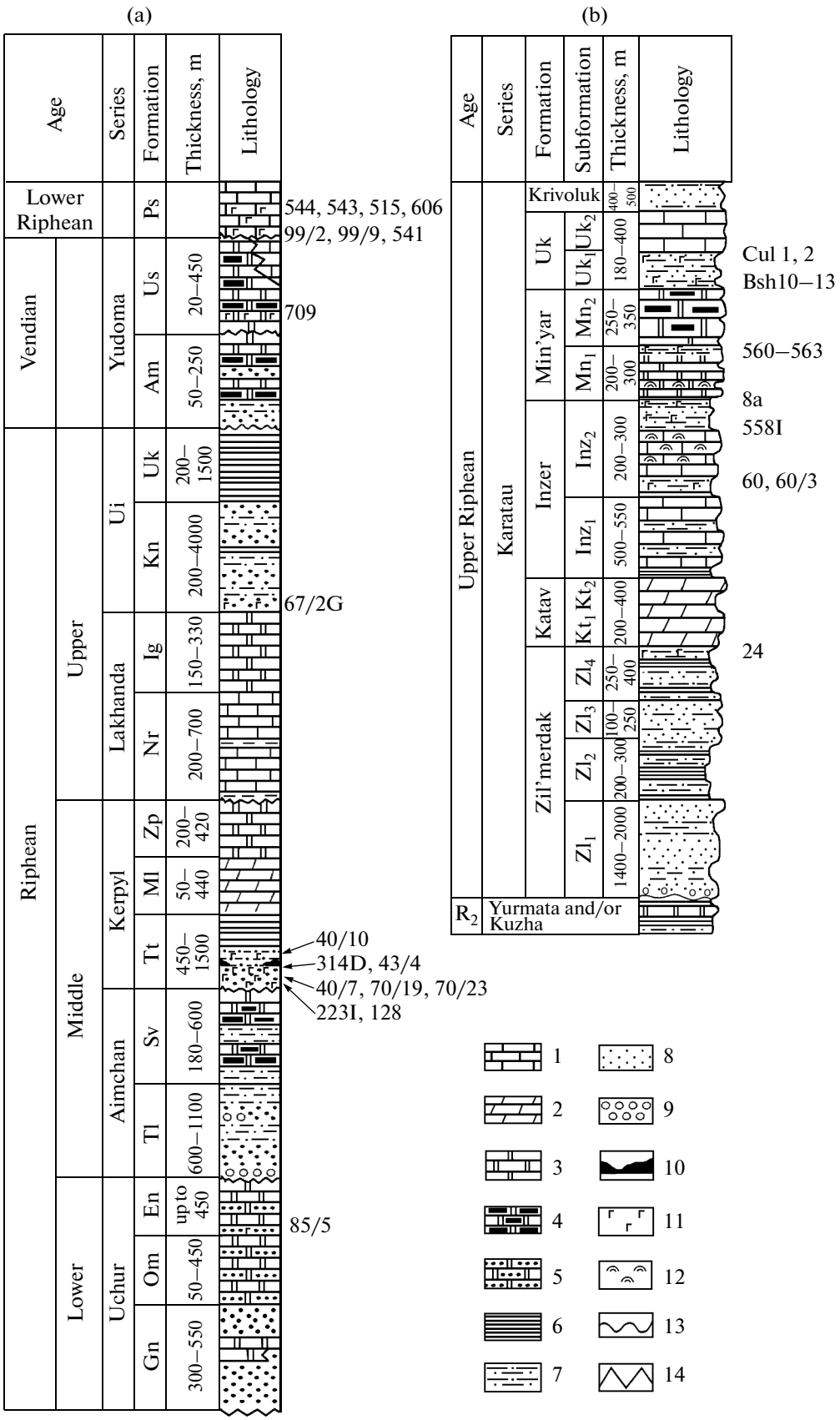
(a)
(b)
Age
Series
Formation
Thickness, m
Lithology
Riphean
Lower Riphean
Vendian
Middle
Upper
Lower
Uchur
Aimchan
Kerpyl
Lakhanda
Ui
Yudoma
Ps
Us
Am
Uk
Kn
Ig
Nr
Zp
Ml
Tt
Sv
Tl
En
Om
Gn
544, 543, 515, 606
99/2, 99/9, 541
709
67/2G
40/10
314D, 43/4
40/7, 70/19, 70/23
223I, 128
85/5
Upper Riphean
Karatau
Zil'merdak
Katav
Inzer
Min'yar
Krivoluk
Uk
Subformation
Cul 1, 2
Bsh10–13
560–563
8a
558I
60, 60/3
24
R2
Yurmata and/or Kuzha
1
2
3
4
5
6
7
8
9
10
11
12
13
14

the formation are divided into three units: the basal unit consisting of sandstones alternating with siltstones and mudstones (6.5–14.5 m thick); the middle unit made up of mudstones with limestone intercalations (21–31 m thick); and the upper siltstone–sandstone unit (18–24 m thick). The rocks frequently contain glauconite (*Vend Podolii*, 1990). Judging from organic remains, the Okunets and Khmel'nitsk formations are ascribed to the Upper Vendian Rovno Horizon according to (Sokolov, 2013).

Samples of sandy–silty rocks with thin intercalations of mudstones were taken from Hole 3652 near the Settlement of Ozhigovtsy (sample 94), from hole near the Settlement of Chukheli (samples 84, 85, 87–90), and from exposures near the Settlement of Kitaigorod (samples 214, 215, 96/2). In the first hole located 8 km west of the second hole, sample 94 was taken from the base of the Khmel'nitsk Formation at a depth from 290.5 to 288.5 m. The second hole was sampled at the base of the formation at a depth of 119.5–116.5 m (samples 84, 85, 87) and upsection within an interval of 108.5–107.5 m (samples 89, 90). In section near the Settlement of Kitaigorod, samples were taken from a 2-m-thick unit at the base of the formation (samples 96/2, 214, 215) (Ivanovskaya, 1996, Fig. 1).

The South Urals

The studied samples belong to the reference Riphean Karatau Group in the western zone of the Bashkirian megantliclinorium, where glauconite-bearing interbeds were found in the following formations (from bottom upward): terrigenous Zil'merdak Formation (1200–3000 m), terrigenous–carbonate Inzer Formation (300–850 m), mainly carbonate Min'yar Formation (350–650 m), and terrigenous–carbonate Uk Formation (180–400 m) that crowns the sequence of the Karatau Group and is unconformably overlain by the Vendian rocks (Figs. 1b, 2b).

Six samples were taken near Min'yar. The section of the Upper Riphean rocks of this region is described in detail in (*Stratotip ripheya*, 1983). In this section, we studied siltstones from the upper part of the Bederysh subformation (Zil'merdak Formation) at the Chernaya Rechka River (sample 24), sandy-clayey rocks on the roof of the Inzer Formation at the Maloyuz Creek (sample 558I), sandstones and siltstones on the roof of the Mink subformation (Min'yar Formation) at the Sim and Min'yar rivers (samples 560, 561, 562, respectively), as well as at the periphery of Min'yar (sample 563). In the Kusa region, we studied the terrigenous–clayey unit supposedly ascribed to the Inzer Formation (samples 60, 60/3). The lower part of variably clayey thin-bedded siltstones yielded sample 60/3; while sample 60 represented by weakly cemented silty mudstone was taken 8 m above the latter sample. Sample 8a was taken from the fragmentary section of the upper part of the Inzer Formation on the Zilim River (Fig. 1b).

The Uk Formation is subdivided into two subformations. In the studied sections, the lower subformation is made up mainly of glauconite–quartz sandstones and siltstones, while the upper part consists of dark gray micritic and stromatolitic limestones. The samples of glauconite sandstones and siltstones were taken from the lower subformation of the Uk Formation near the Settlement of Kurtaza on the Zilim River (samples Bsh10–Bsh13) and near the Settlement of Kulmas on the Basu River (samples Kul1, Kul2) (Fig. 1b). Thickness of the subformation in this section is 110 m and increases to 150 m in the Kulmas section, where the subformation is almost devoid of carbonate rocks. Glauconite is almost ubiquitously developed in the sandy–silty rocks, exceeding 50% in some thin (1–5 cm) interbeds (glauconitite, sample Bsh13) (Zaitseva et al., 2008).

East Siberia

In the Uchur–Maya region, the Siberian Riphean hypostratotype, studied in detail by in (Semikhatov and Serebryakov, 1983), the glauconite-bearing rocks were taken in the Lower Cambrian–Lower Riphean and Middle Riphean sequences recovered by the Mokui Hole (MH) (Ivanovskaya et al., 1985, figure). As mentioned above, the geographic assignment and stratigraphic position of these rocks are shown in Figs. 1c and 2a.

Lower Cambrian. In the sequences recovered along the middle reaches of the Aldan River, the faunally characterized Pestrotsvet Formation (Tommotian Stage) lies with erosional unconformity on rocks of the Vendian Yudoma Group. It is represented by variegated (gray, pink, cherry, and greenish) inequigranular, frequently clayey and locally dolomitized limestones, which often contain glauconite grains. Its thickness is 70–80 m. In the Byukteleekh section, samples were taken at the base of the Pestrotsvet Formation and 0.2–0.3 m upsection (samples 606 and 515, respectively). In the Ulakhan–Sulugur section, samples were

Fig. 2. Stratigraphic position of the studied samples. (a, b) Schematic sections: (a) Riphean, Vendian, and Lower Cambrian of the Uchur-Maya region, (b) Upper Ripnean of the South Urals taken, respectively, from (Sergeev, 2006; Veis et al., 2003) and supplemented by the authors of the present paper. Numbers of studied samples are shown to the right of the sections. Formations: (Gn) Gonam, (Om) Omakhta, (En) Enna, (Tl) Talym, (Sv) Svetlyi, (Tt) Totta, (Ml) Malga, (Zp) Tsipanda, (Nr) Neryuen, (Ig) Ignikan, (Kn) Kandyk, (Uk) Ust-Kurba, (Am) Aim, (Us) Ust-Yudoma, (Ps) Pestrotsvet. ($Є_1$) Lower Cambrian, (R_2) Middle Riphean.(1) Limestone, (2) variegated limestone, (3) dolomite, (4) dolomite with lenses and intercalations of cherts, (5) sandy dolomite, (6) mudstone, (7) siltstone, (8) sandstone, (9) conglomerate, (10) glauconitite interbeds, (11) glauconite, (12) stromatolite, (13) erosions and unconformities, (14) azimuthal unconformities.

taken along strike at the base of the Pestrotsvet Formation (samples 541, 99/2), as well as 0.2–0.3 and 0.8–1.0 m upsection (samples 543, 99/9, and 544, respectively) (Ivanovskaya and Tsipursky, 1982).

Vendian and Upper Riphean. The terrigenous–carbonate Vendian Yudoma Group transgressively rests on the Ui and older rocks and is subdivided into the Aim and Ust-Yudoma formations (Semikhatov and Serebryakov, 1983). In the Yudoma–Maya trough, we sampled the Ust-Yudoma Formation represented mainly by dolomites with intercalations of sandstones, siltstones, and limestones. Thickness of the formation varies from 100–200 to 300–450 m. Dolomite with variably preserved glauconite grains (sample 709) was taken at the base of the Ust-Yudoma Formation at the Yudoma River in the Nuuchalakh section. The Kandyk Formation ascribed to the Upper Riphean Ui Group is made up of alternating sandstones, siltstones, and mudstones. Thickness of the formation in the reference sections varies within 200–4000 m. Glauconite sandstones (sample 67/2G) lie 20m above the base of the formation on the left bank of the Yudoma River (~30 km of the mouth).

Middle Riphean. The Totta Formation is ascribed to the lower part of the Middle Riphean Kerpyl Group. On the northern slope of the Omnya Uplift and within the Maya Basin, it is subdivided into two parts: the lower part (Konder subformation) mainly consisting of sandy sediments and the upper part (Omnya subformation) composed of the finer grained mudstones and siltstones. Thickness of the formation varies from 400–500 to 900–1500 m. Samples were taken at the Omnya Uplift from two sections in the middle part of the Konder subformation: on the left bank (downstream of the Taalakan River mouth) (samples 314D, 40/7) and on the right bank of the Aim River (115 km of the mouth) (sample 43/4). In the first section, sample 314D is located 4.5 m above sample 40/7.

In addition to the indicated samples of the Totta Formation taken along the Aim River, rocks of the same age were studied in the Uchur River (sample 128) on the eastern limb of the Uchur Basin and in the Aldan River (sample 223I) at the Kyllakh Range. Two glauconite-bearing samples from the Totta Formation were taken from the core of MH drilled in the vicinity of the Settlement of Ust-Maya, southeastern Yakutia. They are located at a depth of 2013 to 2035 m: sample 70/19 was taken ~15 m upsection above sample 70/23 (Ivanovskaya et al., 1985).

Lower Riphean. The Lower Riphean Enna Formation in the stratotype section on the right bank of the Uchur River (mouth of the Berdyakit Creek) consists of three sequences: two sandy sequences are separated by the rhythmic terrigenous–carbonate unit. Carbonates are mainly represented by the oncolitic and stromatolitic dolomites. Total thickness of the formation unconformably overlain by the Yudoma rocks reaches 200 m. A unit of inequigranular quartz sandstones with intercalations of glauconite grains is exposed 25 m above the base of the first sequence. Sample 85/5 was taken from the upper part of a 20-m-thick unit (Fig. 2a).

Srednii Peninsula (Murmansk Coast of the Barents Sea)

The Upper Riphean Kil'da Group is subdivided into five subformations. Two lower subformations contain interbeds of grauconite-bearing rocks. The lower interbed is located at the base of the Päräjarvi sandy–silty formation, while the upper interbed occurs at the base of the Palva Formation made up of massive and thin-platy quartz sandstones (Bekker et al., 1970). Glauconite grains from the Päräjarvi Formation are chloritized, whereas glauconite globules in sandstones of the Palva Formation (sample 903/6) were not almost subjected to chloritization, allowing us to calculate its formula (Ivanovskaya et al., 2003).

METHODS

Glauconite grains were separated by our usual procedure, including crushing (except for loose samples), sieving, washing, separation with SEM-1 and SIM-1 electromagnetic separators, and extraction of size fractions in heavy liquids within a density range of 2.4–2.9 g/cm^3 (with a step of 0.05 g/cm^3). Then, the grains were purified in ultrasonic bath and picked with a needle under a binocular microscope.

The extracted grains were studied using the traditional optical, scanning electron microscope (SEM) Stereoskan-600, X-ray diffraction (XRD), and oblique-texture electron diffraction (OTED) methods, as well as the conventional chemical, emission, spectral, and microprobe analyses. The ferrous to ferric ratio in the structure of layer silicates in individual samples was determined by Mössbauer spectroscopy.

The structural–mineralogical analysis of the glauconite-bearing rocks involved the petrographic study of polished thin sections, as well as diffraction (X-ray analysis, OTED) study of clay fractions (<1 and <3 μm) extracted from these rocks. The OTED method was used to analyze separate platy minerals. It should be noted that we also report in this work previously unpublished OTED data (unit cell parameters *b* for mica and chlorite) obtained by C.I. Tsipursky for the finely dispersed and platy minerals from separate samples.

X-ray diffraction. The diffraction patterns of unground and (or) ground globules, as well as their oriented specimens, were obtained on a D8 Advance Bruker diffractometer using CuK_α radiation with the 2θ range from 2.0° to 50.0° for the oriented specimens and from 16.0° to 64.0° for the random specimens.

Oblique-texture electron diffraction, analytical electron microscopy, and local energy-dispersive analysis. Electron diffraction studies of globular layer silicates from East Siberia and South Urals were carried out by S.I. Tsipursky and published in (Ivanovskaya et al., 1989; Tsipursky et al., 1992), and the technique is

described in (Drits et al., 1993). The morphological study of microcrystals, as well as investigation of their selected-area electron diffraction (SAED) patterns and energy-dispersive spectra, were performed using a JEM-100C electron microscope equipped with EDS Kevex-1500. We analyzed only two-phase globules in sample 9/99 (Lower Cambrian Pestrotsvet Formation, Aldan River) (Tsipursky et al., 1992).

Chemical analysis. The complete silicate microanalysis was made for powdered samples (aliquot 300 mg in weight) by the conventional chemical method (analyst K.A. Stepanova). The composition of powdered glauconite grains (aliquot 100 mg in weight) was analyzed using the emission spectroscopy on a JY-48 spectrometer (analyst M.I. Kaikov) (sample 70/19). Microprobe analyses of separate grains placed into a special cartridge were conducted on a Camebax X-ray microanalyzer (analyst G.V. Karpova) (samples 9/99, 94, Kul1, Kul2, Bsh10–Bsh13).

IR spectroscopy. IR absorption spectra of samples Bsh11 and Kul2 were obtained in (Dainyak et al., 2009). IR spectra of samples 541, 70/19, and 60 were obtained using a Bruker VERTEX 80v FTIR spectrometer equipped with a DTGS KBr detector and KBr beam splitter. For each sample, 256 scans were recorded under vacuum in the MIR region (400–4000 cm^{-1}) with a resolution of 4 cm^{-1}. To obtain a KBr pellet, 0.5 mg of sample was dispersed in 200 mg of KBr, the resulting mixture was placed in a 13 mm pellet die and pressed under vacuum for 10–15 min. The pellet was placed into a glass desiccant box with CaCl2 and heated in a furnace at 105°C for at least 20 h.

Spectra manipulations were performed using the OPUS 7.0 software package (Bruker Ltd.). Baseline correction was made automatically using the concave rubber band method with 64 baseline points and 10 iterations.

Mössbauer spectroscopy. The chemical state of Fe in the structure of separate samples was determined by Mössbauer spectroscopy. Spectra were obtained at room temperature on a YaGRS-4 electrodynamic apparatus with constant acceleration using a LP-4840 multichannel analyzer. Sample as cone was mounted at an angle of 54.7° with respect to the γ radiation direction in the Mössbauer spectrometer, which excluded asymmetry of quadrupole splitting doublets related to texturing of the sample (Pfannes and Gonser, 1973; Ericsson and Wäppling, 1976).

CHARACTERISTICS OF THE GLAUCONITE-BEARAING ROCKS

In the Upper Proterozoic and Vendian–Cambrian boundary sequences of the considered regions, the studied samples were taken mainly from sandstones and siltstones thin alternating with mudstones in some places and with dolomites as well in the Mokui Hole section (samples 70/19, 70/23) (Figs. 3a–3c). Among 35 samples, 1 sample represents silty mudstone (sample 60) (Fig. 3d), 1 sample is dolomite (sample 709), and 2 samples are glauconitites (samples 40/7, Bsh13). Ten samples (606, 515, 544, 543, 99/9, 99/2, 607, 1783) were taken from limestones in the Lower Cambrian sequences of East Siberia and the Olenek Uplift (Figs. 3e, 3f).

In terms of texture, structure, mineral composition, and degree of secondary alterations under conditions of deep catagenesis, the sandy–silty rocks are generally close to the previously described Precambrian glauconite-bearing terrigenous rocks of North Siberia (Olenek and Anabar uplifts) (Ivanovskaya et al., 2012). They are parallel- or more rarely, cross-bedded quartz-bearing rocks with admixture of feldspars and mineral plates of different (colorless to dark brown) colors. The plates are made up of dioctahedral Al- and Al–Fe-micas ($b = 9.00–9.05$ Å), trioctahedral chlorite ($b = 9.21–9.25$ Å), and their mineral mixtures. Colorless varieties are represented by illite and Fe-illite with trace chlorite, while brownish flakes contain variable amounts of poorly crystallized trioctahedral chlorite, in addition to dioctahedral micas. In particular, judging from the OTED data, the brown plates in two samples from the Totta Formation in MH are represented by two poorly crystallized phases: Mg–Fe-chlorite ($b = 9.23$, 9.24) and Fe-illite ($b =$ 9.01, 9.04 Å). Chlorite is the predominant component (sample 70/23) and occurs in equal proportions with mica (Ivanovskaya et al., 1985, 1989).

Sandstones and siltstones in the studied sections are characterized by mosaic (conformal-regeneration), scalloped, and rarer scalloped-microstylolitic textures with variable amounts of the clay component represented mainly by the dioctahedral micaceous minerals of variable Al–Fe composition ($b = 9.0–9.06$) along with poorly crystallized trioctahedral Mg–Fe-and Fe–Mg-chlorite ($b = 9.23$, 0.24, and 9.30 Å) (Ivanovskaya et al., 1989, 2003). The clay fractions in the studied glauconite-bearing rocks from the Podolian area also contain micaceous minerals ($b = 9.01–9.03$ Å) and trace chlorite. In addition, they contain an admixture of kaolinite ($b = 8.92–8.94$ Å) (samples 87, 90) and berthierine ($b = 9.32$ Å) (sample 94), which were formed during uplifting of the area (Ivanovskaya, 1996).

As mentioned above, glauconite-bearing mudstones were found only in one of fragmentary sections of the Upper Riphean Inzer (?) Formation, South Urals (sample 60, Fig. 1b). The rocks are weakly cemented. They contain globules (2–3%) and silt-size quartz grains, micaceous flakes of different colors, as well as numerous poorly preserved organic films (Fig. 3d). The clay component in the mudstones is represented by Fe-illite ($b = 9.03$ Å) and insignificant admixture of Mg–Fe^{+2}-chlorite ($b = 9.20$ Å).

Glauconitites as thin interbeds almost completely consisting of glauconite, which occur among dense sandy–silty rocks in the Middle Riphean Totta Formation of East Siberia (sample 40/7) and in the Upper

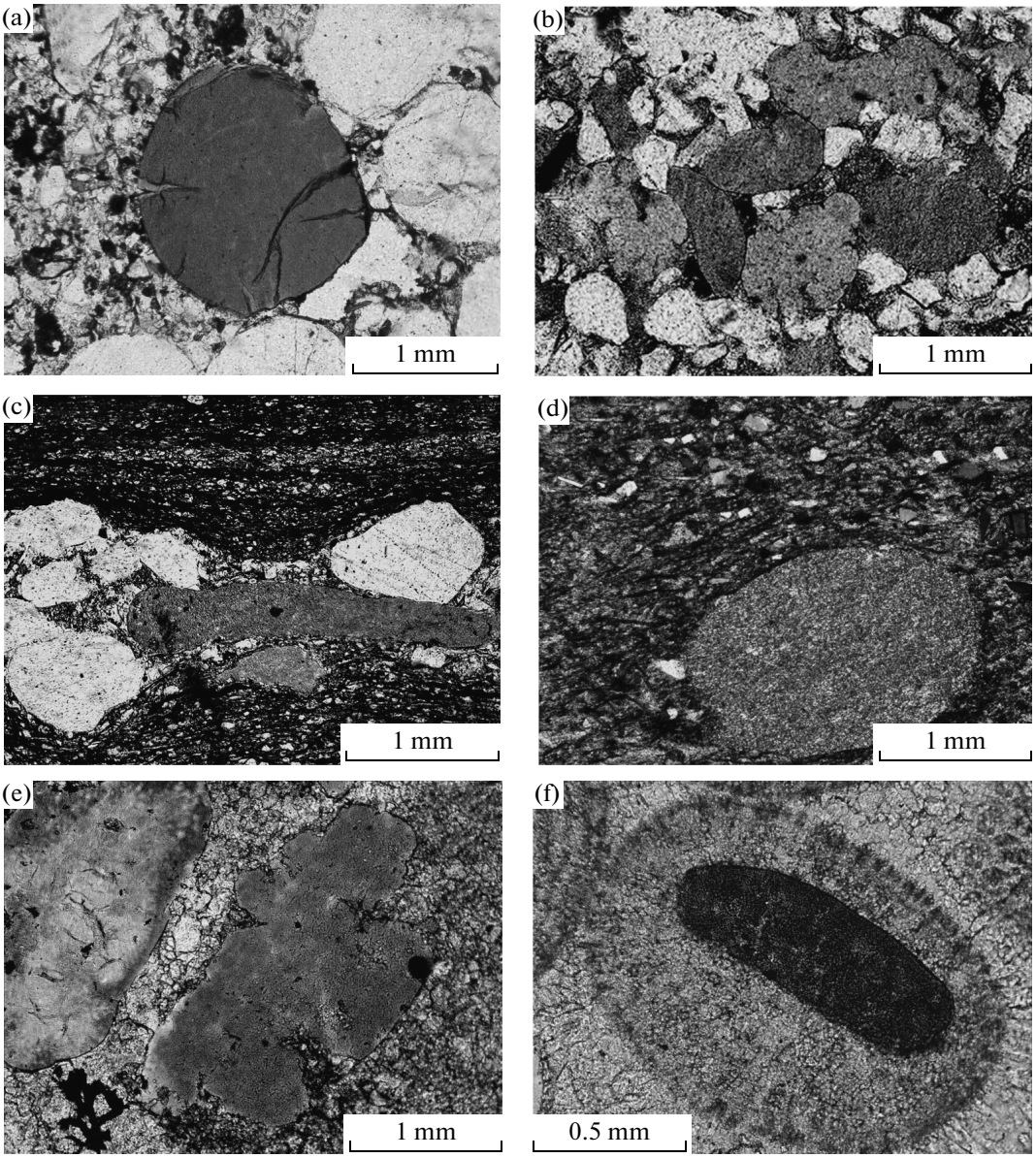

Fig. 3. Grains of layer silicates in different lithologies.(a) Inequigranular sandstone, Totta Formation, East Siberia (sample 341D), (b) siltstone, Totta formation, East Siberia (sample 223I), (c) intercalation of sandstones and mudstones, Totta Formation, Mokui Hole, East Siberia (sample 70/19), (d) mudstones, locally silty, Inzer Formation, South Urals (sample 60), (e) limestone, Pestrotsvet Formation, East Siberia (9/99), (f) oncolitic limestone, Kessyusa Formation, North Siberia (sample 607). Images of polished thin sections:(a–c, e, f) unpolarized light, (d) polarized light.

Riphean Uk Formation of the South Urals (sample Bsh13), are described in detail in (Zaitseva et al., 2008; Ivanovskaya, 2009). Note only that the studied samples represent incoherent or variably cemented green mass consisting mainly of glauconite (as grains and cement) along with quartz and other mineral inclusions.

Dolomites in the Vendian Ust-Yudoma Formation (East Siberia) are represented by light gray inequigranular (from micro- to medium-grained) ornamented, sometimes oncolitic and sandy, varieties. The ornamental fabric of the rock is defined by uneven, locally very intense dolomite recrystallization. The globules of layer silicates are replaced to a variable extent by large (0.6–0.4 mm) rhombohedral dolomite, which contains admixture of quartz, feldspars, and micaceous plates of sand-silt size, as well as hematite and F-apatite. Judging from the mineral and textural features, interbeds of quartz sandstones in the dolomites were also generally transformed under conditions of deep catagenesis, suggesting that the dolomites also experienced a similar degree of secondary alterations.

Limestones developed in the Kessyusa Formation are greenish gray clumpy and oncolitic rocks with glauconite and admixture of terrigenous quartz of sand-silt size (sample 607). In sample 607, glauconite grains frequently occur in both oncolites and the surrounding fine-grained calcite (Fig. 3f). At this stratigraphic level, grains are variably calcitized and often contain inclusions of F-apatite. Limestones of the Pestrotsvet (samples 606, 515, 541, 543, 544, 99/9, 99/2) and Erkeket (sample 1783) formations (Figs. 2a, 3e) have different colors (light green, pink, and cherry). The Erkeket varieties usually have a cherry color. The rocks are inequigranular (micro- to fine-grained) wavy-bedded and massive formations with numerous organic remains.

CHARACTERISTICS OF THE GLAUCONITE–ILLITE GRAINS

As in the previously described collection (Ivanovskaya et al., 2012), the macroscopic and microscopic peculiarities of grains made up of the layer glauconite–illite silicates are somewhat different in the studied samples, but in general are typical of the considered minerals. They form (oval, rounded, nodular, and cerebriform) globules and irregularly shaped segregations of green color of different intensities and tints. Their size varies from 0.63 to 0.2 mm and usually exceeds the size of detrital quartz (Figs. 3a–3c). Glauconitite interbeds contain flattened (sample 40/7) and aggregated grains (sample Bsh13) with small globules cemented by a paler glauconitic mass (Zaitseva et al., 2008, Fig. 3e). Density of grains of different shapes and size varies from 2.45 to 2.85 g/cm^3. Intensity of green color usually increases from the light to heavy fractions. Dark green (up to black) varieties with admixture of F-apatite occur in the heavy fractions of sample 607 (2.75–2.9 g/cm^3).

The morphological and grain-size features of globules in each of the studied sample indicate that they formed in situ in different lithologies. Exception is the oncolitic limestone (sample 607), in which grains are represented by allothigenic varieties. They were subjected to weak erosion and later served as seeds during the formation of oncolites (Fig. 3f).

The study of polished thin sections showed that grains with generally chaotic arrangement of microcrystals are divided into homogenous and heterogeneous varieties (Fig. 3). The homogenous globules are evenly colored and virtually devoid of admixtures. The heterogeneous globules contain inclusions of other minerals and (or) zones, spots, and veins of different green tints. They differ from the groundmass in texture and extinction. In particular, microaggregates contain domains with oriented microcrystals that more frequently occur in deformed varieties, in particular, in rocks subjected to deep catagenetic transformations.

The grains contain inclusions of dolomite (sample 709), calcite (samples 607, 1783, 314D, 40/7), F-apatite (samples 709, 607), and iron hydroxides (samples 709, 40/7, 85/5, 128, and 563). In spite of the fact that we analyzed mainly homogenous varieties, some samples are dominated by grains with inclusions of different minerals (samples 607, 709, 85/5), but they were identified during the complete silicate microanalysis and were subtracted in calculation of the crystal-chemical formula.

The SEM study of the outer and inner surfaces of globules of layer silicates shows that, regardless of composition (glauconite, Al-glauconite, Fe-illite, or illite), they are made up of gently bending and variably oriented microcrystals from 1 or 2 to 4 or 5 μm in size (Fig. 4), which could be grouped to form peculiar clusters. In particular, glauconite grains in sample 99/9 (Lower Cambrian, Aldan River) are characterized by imbricate-flaky (locally oriented) microstructure (Figs. 4d, 4e). In some places, they contain accumulations of crystals resembling "sand roses" (Fig. 4f) similar to those in young sediments (Odin, 1974).

STRUCTURAL AND CRYSTAL-CHEMICAL FEATURES OF THE STUDIED SAMPLES

Cation Composition of Micaceous Minerals

Crystal-chemical formulas of globular layer silicates were calculated for the anion framework $O_{10}(OH)_2$ using the wet chemical and microprobe analyses, as well as the results of emission spectral analysis. Chemical analyses of 45 samples (65 fractions) were taken from (Ivanovskaya and Tsipursky, 1982; Ivanovskaya et al., 1989, 2003; Tsipursky et al., 1992; Ivanovskaya, 1996; Zaitseva et al., 2008) and reported for the first time for samples 607 and 1783.

The studied layer silicates show wide variations in the content of tri- and bivalent cations in the octahedral sheets of 2 : 1 layers: Al 1.46–0.16, Fe^{3+} – 1.35–0.13, Fe^{2+} 0.37–0.04, Mg 0.75–0.21 f.u. (Table 1). According to IMA NC and AIPEA NC classifications (Rieder et al., 1998; Guggenheim et al., 2006) and classification in (Kossovskaya and Drits, 1971), based on the isomorphic substitution of Fe^{3+} and Al^{3+} in octahedra, the studied samples are subdivided into glauconites (10 samples, 12 fractions), Al-glauconites (7 samples, 11 fractions), Fe-illites (21 samples, 31 fractions), and illites (7 samples with $^{VI}Al/(^{VI}Al + {}^{VI}Fe^{3+})$ = 0.11–0.50, 0.51–0.58, 0.61–0.78, and 0.81–0.91, respectively. Figure 5 demonstrates variations of $R^{2+}/(R^{2+} + R^{3+})$ (where R^{2+} and R^{3+} are the total content of the bi- and trivalent cations, respectively) versus $^{VI}Al/(^{VI}Al + {}^{VI}Fe^{3+})$ ratio in the glauconite and illite fields determined by IMA NC and approved by INC on clay minerals (AIPEA NC) (Fieder et al., 1998; Guggenheim et al., 2006). The cation compositions of the studied silicates of the glauconite–illite composition not always fall into these fields. In particular, they contain intermediate varieties (Al-glauconites), while $R^{2+}/(R^{2+} + R^{3+})$ in

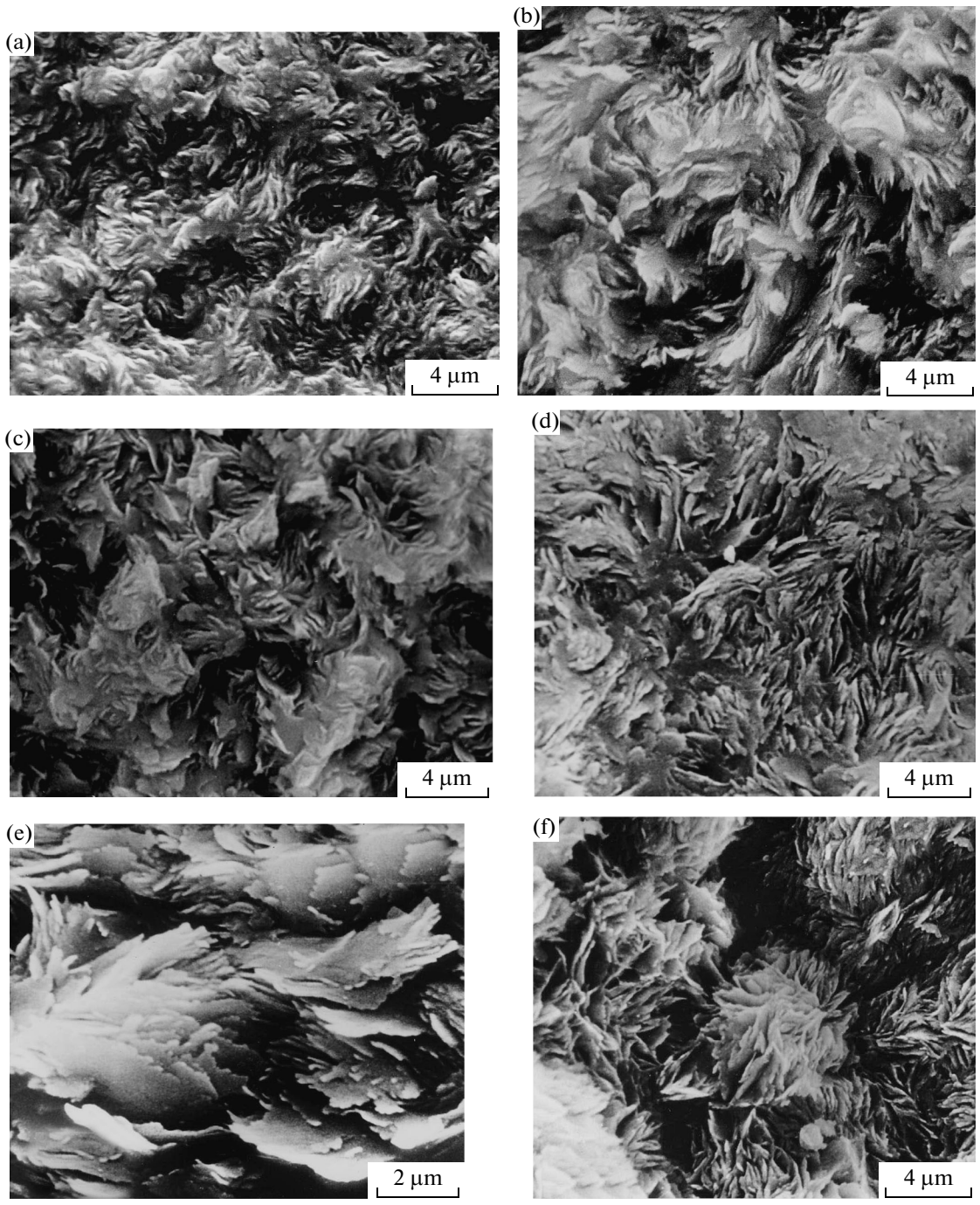

Fig. 4. Microtexture of the inner (a–c, e, f) and outer (d) surface of the globules of different compositions. (a) Al-glauconite (sample 43/4), (b) Fe-illite (sample Bsh10), (c) illite (sample 60), (d–f) glauconite (sample 99/9). SEM.

illites (up to 0.47) exceeds the value accepted by IMA NC (≤0.25) (Rieder et al., 1998). According to classification (Kossovskaya and Drits, 1971; Drits et al., 2013), we distinguish Fe-illites (K_{Al} = 0.6–0.8) and preserve the term "Al-glauconite" for varieties with K_{Al} ranging from 0.51 to 0.59 (Ivanovskaya et al., 2013, Ivanovskaya and Zaitseva, 2015).

In addition to isovalent isomorphism of Fe^{3+} and Al^{3+}, the studied samples show heterovalent isomorphism in the octahedral (Fe^{3+}, Al, Mg, Fe^{2+}) and tetrahedral (Si^{4+}, Al^{3+}) sheets of 2 : 1 layers, which determines the total negative charge of 2 : 1 layer. The total charge of 2 : 1 layer varies from 0.64 to 0.92 and is balanced by interlayer K (K = 0.56–0.85 f.u.) and minor

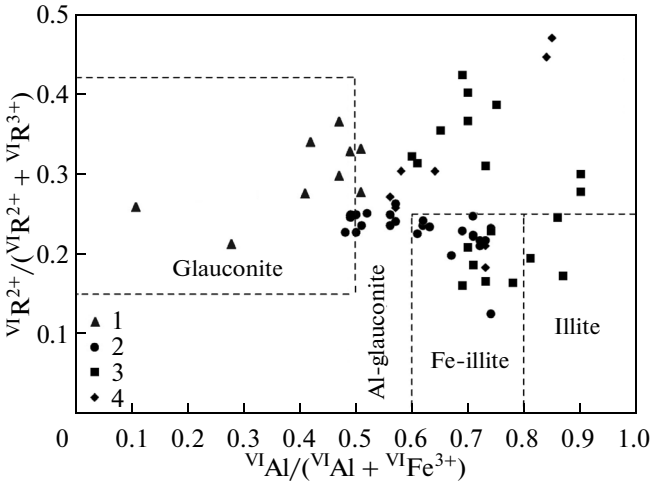

Fig. 5. Correlation between $R^{2+}/(R^{2+} + R^{3+})$, where R^{2+} and R^{3+} are the total contents of bi- and trivalent cations), and $^{VI}Al/(^{VI}Al + {}^{VI}Fe^{3+})$ for the studied globular layer silicates within fields determined by IMA NC for glauconites and illites (Rieder et al., 1998). Age: (1) Lower Cambrian (Olenek Uplift, East Siberia), (2) Vendian–Lower Cambrian beds (Podolian Dniester region), (3) Vendian and Upper Riphean (East Siberia, South Urals, Srednii Peninsula), (4) Middle and Lower Riphean (East Siberia).

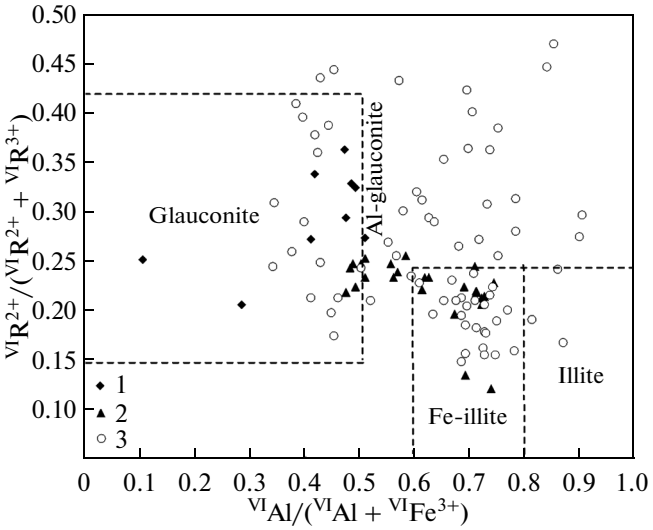

Fig. 6. Correlation between $R^{2+}/(R^{2+} + R^{3+})$ and Al index $^{VI}Al/(^{VI}Al + {}^{VI}Fe^{3+})$ within the fields determined by IMA NC for glauconites and illites for the dioctahedral micaceous minerals studied in (Ivanovskaya et al., 2012) and this paper. Age: (a) Lower Cambrian, (2) Vendian–Cambrian boundary beds, (3) Upper Proterozoic.

amounts of Ca and Na cations. In terms of the K content, the globular layer silicates belong to low-charge micaceous minerals. The lowest contents of this cation (K = 0.56, 0.59 f.u.) were found in some fractions of samples 89 and 90 (Podolian Dniester region) (Table 1, an. 19, 25). In other samples (and other fractions of samples 89, 90), the number of K cations in layer silicates varies from 0.6 to 0.85 f.u. (Table 1).

Crystal-chemical data on 79 samples of globular layer silicates of the glauconite–illite composition obtained previously (Ivanovskaya et al., 2012) and presented in this paper are shown in Fig. 6. The wide variations of the tri- and bivalent cations in the octahedral sheets of 2 : 1 layers make it possible to distinguish, as mentioned above, a continuous isomorphic series from illites via Fe-illites and Al-glauconites to glauconites (K_{Al} = 0.8–0.91, 0.6–0.8, 0.51–0.59, and 0.11–0.50, respectively). The interlayer charge in the low-charge micaceous minerals varies mainly from 0.63 to 0.87 at the K cation content of 0.6–0.85 f.u. The studied phyllosilicates are dominated by Fe-illites (45 samples); illites and Al-glauconites (7 and 10 samples, respectively) are less common; and glauconites occur in 17 samples. Compositional variations of the studied mineral varieties fall beyond the boundaries accepted by INC on micas (IMA NC) and approved by INC on clay minerals (AIPEA NC) (Fig. 6).

The X-Ray Diffraction Data

Peculiarities of X-ray diffraction patterns of oriented specimens. The X-ray diffraction (XRD) patterns recorded from natural and glycolated specimens are typical of micaceous minerals. The most intense peaks of the first five basal reflections are 001 and 003. Diffraction features of samples in natural and saturated states are similar to those obtained previously for the collection of globular layer silicates from North Siberia (Ivanovskaya et al., 2012). Their structural varieties were distinguished on the basis of criteria in (Drits et al., 1993).

In this paper, we determined the contents of expandable layers in the structure of micaceous minerals, their alternation (short-range order factor R) and parameters $c\sin\beta$ of mica layers in 27 glycolated samples by simulating diffraction patterns (Sakharov et al., 1999) (Table 2). The studied samples can be divided into two groups with relatively low and high contents of expandable layers (4–8 and 10–13%) (Table 2). In the first group (13 samples), the diffraction patterns recorded from natural specimens show an almost integral series of basal reflections, except for the first low-angle reflections with d = 10.11–10.22 Å, the high values of which are determined by the interstratification effect and small crystal sizes. The saturation of specimens with ethylene glycol results in a slight shift of 001 reflection toward larger angles 2θ (d(001) = 9.92–10.05 Å). In addition, the intensity of 001 reflection slightly decreases as compared to that in the XRD pattern of natural specimens. Such diffraction features

Table 1. Crystal-chemical formulas of layer silicates of the glauconite–illite composition

Analysis no.	Sample no.	Grain size, mm	Density, g/cm^3	Cations										$^{VI}Al/(^{VI}Al+^{VI}Fe^{3+})$	Charges			Fe^{2+}/Fe^{3+}
				tetrahedral		octahedral					interlayer				tetrahedral	octahedral	interlayer	
				Si	Al	Al	Fe^{3+}	Fe^{2+}	Mg	Σ_{oct}	K	Na	Ca					
Lower Cambrian (Olenek Uplift, East Siberia)																		
1	1783	0.63–0.2	2.6–2.7	3.64	0.36	0.45	1.12	0.10	0.32	1.99	0.75	0.04	–	0.29	15.64	5.55	0.79	0.09
2	607	0.4–0.2	2.7–2.9	3.64	0.36	0.16	1.35	0.22	0.30	2.03	0.67	0.06	0.02	0.11	15.64	5.57	0.77	0.16
3	515	0.16–0.1	2.75–2.8	3.58	0.42	0.61	0.87	0.09	0.47	2.04	0.78	0.02	0.03	0.41	15.58	5.56	0.86	0.10
4	606	0.16–0.1	2.7–2.75	3.64	0.36	0.68	0.70	0.17	0.50	2.05	0.85	–	0.02	0.49	15.64	5.48	0.89	0.24
5	544	0.1–0.063	2.75–2.8	3.68	0.32	0.57	0.79	0.21	0.49	2.06	0.70	0.02	0.06	0.42	15.68	5.48	0.84	0.27
6	543	0.16–0.1	2.75–2.85	3.59	0.41	0.76	0.73	0.20	0.37	2.06	0.78	0.01	–	0.51	15.59	5.61	0.79	0.27
General crystal-chemical formula of two-phase sample 99/9 (an. 7) and compositions of individual phases (an. 8, 9) in globules																		
7	99/9*	0.4–0.2	2.65–2.75	3.59	0.41	0.86	0.55	0.28	0.31	2.00	0.82	–	0.02	0.61	15.59	5.41	0.86	0.51
8	99/9	0.4–0.2	2.65–2.75	3.74	0.26	0.60	0.67	0.43	0.30	2.00	0.82	–	0.02	0.47	15.74	5.27	0.86	0.64
9	99/9	0.4–0.2	2.65–2.75	3.30	0.70	1.35	0.33	–	0.32	2.00	0.82	–	0.02	0.80	15.30	5.68	0.86	–
10	99/2	0.2–0.1	2.65–2.75	3.56	0.44	0.70	0.77	0.23	0.39	2.09	0.78	–	0.02	0.48	15.56	5.65	0.82	0.30
11	541*	0.4–0.2	2.7–2.8	3.53	0.47	0.68	0.72	0.29	0.40	2.09	0.78	0.01	0.06	0.49	15.53	5.58	0.91	0.40
Vendian--Lower Cambrian boundary beds (Podolian Dniester region)																		
12	84*	0.25–0.16	2.7–2.75	3.69	0.31	0.77	0.76	0.26	0.25	2.04	0.62	0.02	0.04	0.50	15.69	5.61	0.72	0.34
13	84	0.25–0.16	2.75–2.8	3.64	0.36	0.74	0.82	0.19	0.26	2.01	0.66	0.02	0.04	0.47	15.64	5.58	0.76	0.23
14	85	0.5–0.25	–	3.67	0.33	0.74	0.79	0.23	0.27	2.03	0.65	0.01	0.04	0.48	15.67	5.59	0.74	0.29
15	85	0.25–0.16	2.75–2.8	3.66	0.34	0.77	0.79	0.19	0.27	2.02	0.66	0.02	0.04	0.49	15.66	5.60	0.76	0.24
16	87	0.25–0.16	2.7–2.75	3.71	0.29	0.87	0.68	0.21	0.27	2.03	0.61	0.02	0.03	0.56	15.71	5.61	0.69	0.31
17	87*	0.25–0.16	2.75–2.8	3.68	0.32	0.77	0.74	0.24	0.28	2.03	0.65	0.02	0.04	0.51	15.68	5.57	0.75	0.32
18	87	0.16–0.1	2.75–2.8	3.67	0.33	0.84	0.67	0.23	0.28	2.02	0.63	0.02	0.05	0.56	15.67	5.55	0.75	0.34
19	89	0.5–0.2	2.7–2.75	3.75	0.25	0.96	0.59	0.19	0.29	2.03	0.56	0.02	0.03	0.62	15.75	5.61	0.64	0.32
20	89	0.5–0.2	2.75–2.8	3.69	0.31	0.87	0.66	0.20	0.29	2.02	0.65	0.02	0.03	0.57	15.69	5.57	0.73	0.30
21	89	0.2–0.16	2.65–2.7	3.67	0.33	0.96	0.59	0.20	0.28	2.03	0.63	0.02	0.04	0.62	15.67	5.61	0.73	0.34

Table 1. (Contd.)

Analysis no.	Sample no.	Grain size, mm	Density, g/cm^3	Cations										$^{VI}Al/(^{VI}Al+^{VI}Fe^{3+})$	Charges			Fe^{2+}/Fe^{3+}
				tetrahedral		octahedral					interlayer				tetrahedral	octahedral	interlayer	
				Si	Al	Al	Fe^{3+}	Fe^{2+}	Mg	Σ_{oct}	K	Na	Ca					
22	89*	0.2–0.16	2.7–2.75	3.73	0.27	0.88	0.63	0.25	0.28	2.04	0.63	0.01	0.02	0.58	15.73	5.59	0.68	0.40
23	89	0.2–0.16	2.75–2.8	3.70	0.30	0.79	0.76	0.19	0.29	2.03	0.64	0.01	0.02	0.51	15.70	5.61	0.69	0.25
24	90	0.25–0.16	2.65–2.7	3.66	0.34	0.97	0.58	0.16	0.32	2.03	0.66	0.02	0.02	0.63	15.66	5.61	0.72	0.28
25	90	0.16–0.07	2.65–2.7	3.68	0.32	0.95	0.60	0.18	0.27	2.00	0.59	0.02	0.07	0.61	15.68	5.55	0.75	0.30
General crystal-chemical formula of micaceous minerals of Fe- and Al- composition in the globules from sample 94 (an. 26) and individual compositions of globules (an. 27, 28)																		
26	94	0.315–0.2	2.7–2.75	3.64	0.36	0.88	0.67	0.19	0.26	2.00	0.74	–	0.02	0.57	15.64	5.55	0.78	0.28
27	94	0.315–0.2	2.7–2.75	3.68	0.32	0.73	0.77	0.23	0.27	2.00	0.73	–	0.02	0.49	15.68	5.50	0.77	0.30
28	94	0.315–0.2	2.7–2.75	3.50	0.50	1.33	0.35	0.08	0.23	1.99	0.78	–	0.02	0.79	15.50	5.66	0.82	0.23
29	214	0.5–0.25	2.6–2.65	3.73	0.27	1.16	0.40	0.18	0.29	2.03	0.64	0.01	–	0.74	15.73	5.62	0.65	0.45
30	214*	0.5–0.25	2.65–2.7	3.73	0.27	1.07	0.44	0.20	0.30	2.01	0.70	0.01	0.01	0.71	15.73	5.53	0.73	0.45
31	214	0.25–0.16	2.6–2.65	3.65	0.35	1.15	0.43	0.17	0.27	2.02	0.69	0.00	0.02	0.73	15.65	5.62	0.73	0.40
32	214	0.25–0.16	2.65–2.7	3.70	0.30	1.14	0.44	0.16	0.26	2.00	0.63	0.01	0.04	0.72	15.70	5.58	0.72	0.36
33	214	0.16–0.07	2.6–2.65	3.65	0.35	1.14	0.44	0.16	0.28	2.02	0.65	0.01	0.02	0.72	15.65	5.62	0.72	0.36
34	214	0.16–0.07	2.65–2.7	3.66	0.34	1.11	0.45	0.18	0.27	2.01	0.68	0.00	0.03	0.71	15.66	5.58	0.74	0.40
35	214	0.16–0.07	2.7–2.75	3.69	0.31	1.07	0.48	0.19	0.27	2.01	0.65	0.01	0.04	0.69	15.69	5.57	0.74	0.40
36	215	0.25–0.16	2.6–2.65	3.71	0.29	1.11	0.45	0.17	0.28	2.01	0.65	0.01	0.02	0.71	15.71	5.58	0.70	0.38
37	96/2	0.315–0.2	2.6–2.65	3.59	0.41	1.28	0.45	0.04	0.21	1.98	0.65	0.01	0.03	0.74	15.59	5.69	0.72	0.09
38	96/2	0.315–0.2	2.65–2.7	3.49	0.51	1.11	0.54	0.12	0.29	2.06	0.66	0.02	0.04	0.67	15.49	5.77	0.76	0.22
Vendian and Upper Riphean (East Siberia, South Urals, Srednii peninsula)																		
39	709	0.16–0.1	2.5–2.75	3.57	0.43	0.90	0.48	0.11	0.65	2.14	0.75	0.02	–	0.65	15.57	5.66	0.77	0.23
40	67/2G*	0.4–0.2	2.55–2.61	3.61	0.39	1.46	0.22	0.10	0.25	2.03	0.60	0.02	0.01	0.87	15.61	5.74	0.64	0.45
41	Kul1*	0.315–0.2	2.7–2.75	3.75	0.25	0.92	0.40	0.38	0.38	2.08	0.75	–	0.01	0.70	15.75	5.48	0.77	0.95
42	Kul2*	0.2–0.16	2.6–2.7	3.72	0.28	0.84	0.55	0.26	0.40	2.05	0.77	–	0.02	0.60	15.72	5.49	0.81	0.47
43	Kul2*	0.315–0.2	2.7–2.75	3.72	0.28	0.86	0.54	0.25	0.39	2.04	0.76	–	0.02	0.61	15.72	5.48	0.80	0.46
44	Bsh10*	0.25–0.16	2.7–2.8	3.73	0.27	0.84	0.37	0.37	0.52	2.10	0.79	–	0.02	0.69	15.73	5.41	0.83	1.00
45	Bsh11*	0.25–0.2	2.6–2.7	3.69	0.31	1.04	0.38	0.22	0.42	2.06	0.74	–	0.02	0.73	15.69	5.54	0.78	0.58
46	Bsh12*	0.25–0.2	2.7–2.75	3.73	0.27	0.88	0.37	0.37	0.47	2.09	0.78	–	0.02	0.70	15.73	5.43	0.82	1.00

Table 1. (Contd.)

Analysis no.	Sample no.	Grain size, mm	Density, g/cm^3	Cations										$^{VI}Al/(^{VI}Al+^{VI}Fe^{3+})$	Charges			Fe^{2+}/Fe^{3+}
				tetrahedral		octahedral					interlayer				tetrahedral	octahedral	interlayer	
				Si	Al	Al	Fe^{3+}	Fe^{2+}	Mg	Σ_{oct}	K	Na	Ca					
47	Bsh13*	0.4–0.315	2.65–2.7	3.70	0.30	0.97	0.32	0.29	0.52	2.10	0.74	–	0.02	0.75	15.70	5.49	0.78	0.91
48	563	0.1–0.063	–	3.42	0.58	1.19	0.53	0.08	0.25	2.05	0.70	0.01	0.02	0.69	15.42	5.82	0.75	0.15
49	562	0.1–0.063	2.45–2.7	3.58	0.42	1.31	0.37	0.10	0.23	2.01	0.66	0.01	0.02	0.78	15.58	5.70	0.71	0.27
50	561	0.1–0.063	–	3.48	0.52	1.24	0.47	0.08	0.26	2.05	0.70	0.01	–	0.73	15.48	5.81	0.71	0.17
51	560	0.1–0.063	–	3.45	0.55	1.18	0.48	0.13	0.25	2.04	0.73	0.01	0.03	0.71	15.45	5.74	0.80	0.27
52	558I	0.1–0.063	2.5–2.75	3.48	0.52	1.14	0.50	0.17	0.26	2.07	0.74	0.01	–	0.70	15.48	5.78	0.75	0.34
53	8a	0.1–0.063	2.7–2.75	3.50	0.50	1.18	0.41	0.08	0.39	2.06	0.75	0.01	–	0.74	15.50	5.71	0.76	0.20
54	60*	0.315–0.2	2.6–2.7	3.63	0.37	1.32	0.13	0.16	0.45	2.06	0.79	0.01	–	0.91	15.63	5.57	0.80	1.23
55	60/3*	0.16–0.1	2.65–2.7	3.64	0.36	1.34	0.13	0.15	0.40	2.02	0.81	0.01	0.02	0.91	15.64	5.51	0.86	1.15
56	24	0.1–0.063	2.6–2.7	3.53	0.47	1.34	0.31	0.14	0.26	2.05	0.63	0.03	0.03	0.81	15.53	5.75	0.72	0.45
57	903/6*	0.5–0.16	2.4–2.65	3.68	0.32	1.30	0.21	0.20	0.29	2.00	0.78	–	–	0.86	15.68	5.51	0.78	0.95
Middle and Lower Riphean (East Siberia)																		
58	43/4*	0.63–0.315	2.6–2.65	3.59	3.41	0.84	0.68	0.19	0.38	2.09	0.67	0.01	0.02	0.55	15.59	5.70	0.72	0.28
59	314D*	0.315–0.2	2.55–2.65	3.64	0.36	0.92	0.55	0.25	0.37	2.09	0.67	0.02	0.01	0.63	15.64	5.65	0.71	0.45
60	40/7*	0.315–0.2	2.6–2.7	3.67	0.33	0.86	0.66	0.23	0.30	2.05	0.65	0.03	0.02	0.57	15.67	5.62	0.72	0.35
61	128*	0.315–0.2	2.6–2.7	3.56	0.44	1.20	0.45	0.10	0.27	2.02	0.67	0.02	0.03	0.73	15.56	5.69	0.75	0.22
62	223I*	0.16–0.1	2.65–2.75	3.40	0.60	1.20	0.45	0.21	0.23	2.09	0.73	0.01	0.01	0.73	15.40	5.83	0.76	0.47
63	70/23*	0.4–0.2	2.65–2.75	3.74	0.26	1.00	0.19	0.29	0.67	2.15	0.77	0.01	–	0.84	15.74	5.49	0.78	1.53
64	70/19	0.4–0.2	2.7–2.8	3.73	0.27	0.98	0.17	0.27	0.75	2.17	0.80	–	0.01	0.85	15.73	5.49	0.82	1.59
65	85/5*	0.4–0.315	2.75–2.8	3.74	0.26	0.80	0.58	0.12	0.48	1.98	0.84	0.02	0.03	0.58	15.74	5.34	0.92	0.21

Formulas 8 and 9 are Fe- and Al-phases from sample 99/9. Their proportions in individual globules are 65 and 35%, respectively (Tsipursky et al., 1992). Formulas 27 and 28 are Fe- and Al-phase compositions of dark green globules in a single fraction of sample 94, in which the proportions of globules of different compositions are 75 and 25%, respectively (Ivanovskaya et al., 1999). (*) Fe^{2+}/Fe^{3+} ratio given by the Mössbauer data. In formulas 12–14, 17, 18, 20–24, 54, 55, 58–60, the K content was recalculated according to analyses presented in (Semikhatov et al., 1987; Gorokhov et al., 1997). Dash means data are absent.

are typical of glauconite (samples 515, 544, 543, 541, 99/9), Al-glauconite (sample 85/5), Fe-illite (samples Kul1, Bsh10–Bsh12), and illite (samples 709, 60/3, 70/19) (Table 1).

The second group (14 samples) is marked by the higher d value of the first low-angle basal reflection (10.28–10.65 Å) and more significant violation of the integrity of basal reflection series. Ethylene glycol saturation in some samples (samples 60, 314D) results in the appearance of one symmetrical reflection 001 in the low-angle region, which is shifted toward high 2θ angles. Its d values vary from 9.94 to 9.99 Å. In other samples (samples 87, 89, 214, 96/2, 67/2G, 8a, 24, 40/7, 43/4, 128, and 223I), this region shows either reflection asymmetrical toward the low angles or its splitting into two reflections with d = 10.7–11.34 Å and d = 9.67–9.94 Å, indicating a tendency to the ordered alternation of layers of different types (R ≥ 1). In terms of composition, the studied samples belong to Al-glauconite (samples 87, 89, 40/7, 43/4), Fe-illite (samples 214, 96/2, 8a, 128, 223I, 314D) and illite (samples 60, 67/2g, 24) (Table 1).

The short-range order factor R is defined as the number of preceding layers that determine the probability of appearance of the given layer in a mixed-layer structure. If layers of different types show disordered alternation, the occurrence of a layer of the given type in any position in the structure does not depend on the nature of the adjacent layers and R = 0. If the probability of the layer occurrence depends on one previous layer, R = 1. If this probability depends on two previous layers, then R = 2 and so on.

Simulation of experimental diffraction patterns showed that the degree of short-range order in the alternation of layers of different types in the studied samples varies (R = 0, 2, and 3) (Table 2). Best fit between the calculated and experimental diffraction patterns was reached in models based on one (16.85 Å) or two (16.85 Å and ~12.9–13.2 Å) types of expandable layers. Layers ~12.9–13.2 Å in thickness are ascribed to the vermiculite-type or high-charge smectite components. As an example, Figs. 7a–7c demonstrate the calculated and experimental diffraction patterns of oriented glycolated specimens corresponding to the three- and two-component mixed-layer structures with R = 3, 2, and 0 (samples 67/2G, 89, and 10Bsh, respectively). As seen in Table 2, the three-component mixed-layer structures (mica–smectite–vermiculite) occur in 12 samples (samples 515, 89, 214, 67/2G, 8a, 24, 40/7, 43/4, 314D, 128, 223I, 85/5), which are represented by mineral varieties ranging from glauconite via Al-glauconite and Fe-illite to illite (Table 1). The alternation of layers of different types in such structures can be disordered (R = 0) or have a trend to ordering (R = 2 and 3).

It should be noted that the structure of three samples of Al-glauconites (samples 314D, 43/4, 40/7) from sandstones in two sections of the middle part of the Konder subformation of the Totta Formation (Aim River) (Fig. 3a) is characterized by different degrees of the ordering of mica, smectite, and vermiculite layers (R = 0 and 2, 3) (Table 2, an. 33–35). The differences in the degree of short-range order in the alternation of different layers in the structure of the studied samples is presumably caused by different conditions of microcrystal growth in non-equilibrium mineral formation environment rather than the catagenetic transformation of host rocks. The presence of globular layer silicates of the glauconite–illite composition characterized by the ordered alternation of mica and smectite layers was also noted in the weakly altered Lower Cretaceous sandy–silty sediments of England (Geptner and Ivanovskaya, 2000).

Features of the powder XRD patterns. Interpretation of powder diffraction patterns of the studied glauconite–illite layer silicates is based on criteria in (Drits et al., 1993). Below, we report the analysis of diffraction patterns of random specimens of the studied samples.

Based on the degree of resolution and broadening of reflections 02*l* and 11*l*, the studied samples can be subdivided into three groups marked by high, middle, and low degree of the three-dimensional ordering. Reflections $\bar{1}12$ and 112 are most sensitive to the degree of structural ordering (content of stacking faults). Their intensity gradually decreases with increasing number of stacking faults of any type.

The profile and intensity of reflections $\bar{1}11$ and 021 (as comared with those of 020 and 110) can serve as additional criteria for the degree of 3D ordering of dioctahedral layer silicates. In samples with high degree of 3D ordering, reflections $\bar{1}11$ and 021 are well resolved; the second group is characterized by a lower intensity of reflection $\bar{1}11$ and low-intensity broad reflection 021. In the third group, these reflections are almost absent.

Only samples from the Totta Formation in East Siberia (samples 223I, 314D) (Sakharov et al., 1990) and Inzer Formation in the South Urals (sample 60) were studied previously based on the modeling of experimental diffraction patterns recorded from random specimens (Drits et al., 2013). In particular, sample 60 is characterized by sharp and intense reflections 11*l* and 20*l*, which allowed us to identify it as a mica with a relatively high degree of structural ordering. The diffraction pattern of sample 223I shows less intense and broad reflections $\bar{1}12$ and 112 with d = 3.654 and 3.074 Å, weak reflection $\bar{1}11$ with d ~ 4.37 Å, and a minor shoulder (reflection 021) in the region d ~ 4.12 Å. Similar pattern is typical of samples with the moderate degree of ordering. The region of reflections 02*l* and 11*l* in the powder diffraction pattern of sample 314D contains only weak reflections $\bar{1}12$ and 112, indicating that its structure has a low degree of 3D ordering.

Table 2. XRD data on globular layer silicates of the glauconite–illite composition

Analysis no.	Sample no.	Grain size, mm	Density, grain, g/cm^3	Expandable layers, %		Factor *R*	d (060), Å	Parameter *b*, Å	c sin β
				Sm	Verm				
1	515	0.16–0.1	2.75–2.8	6	2	0	1.515, 1.497	9.090, 8,98	9.99
2	544	0.1–0.063	2.75–2.8	5	–	0	1.515, 1.498	9.090, 8.99	10.0
3	543	0.16–0.1	2.75–2.85	5	–	0	1.517, 1.501	9.102, 9.01	10.0
4	541	0.4–0.2	2.7–2.8	5	–	0	1.513, 1.498	9.078, 8.99	9.99
5	99/9	0.4–0.2	2.65–2.75	7	–	0	1.513, 1.497	9.078, 8.98	9.985
6	607	0.4–0.2	2.7–2.9	–	–	–	1.518	9.108	–
7	1783	0.63–0.2	2.6–2.7	–	–	–	1.515	9.090	–
8	87	0.25–0.16	2.7–2.75	–	–	–	1.514	9.084	–
9	87	0.25–0.16	2.75–2.8	13	–	2	1.514	9.084	9.99
10	89	0.20–0.16	2.65–2.7	–	–	–	1.512	9.072	–
11	89	0.20–0.16	2.7–2.75	–	–	–	1.513	9.078	–
12	89	0.20–0.16	2.75–2.8	10	3	2	1.514	9.084	9.99
13	90	0.25–0.16	2.65–2.7			–	1.510	9.060	–
14	214	0.5–0.25	2.6–2.65	8	2	3	1.506	9.036	9.98
15	214	0.5–0.25	2.65–2.7	10	1	3	1.510	9.060	9.98
16	215	0.25–0.16	2.6–2.65	–	–	–	1.509	9.054	9.98
17	96/2	0.315–0.2	2.6–2.65	–	–	–	1.507	9.042	–
18	96/2	0.315–0.2	2.65–2.7	12	–	2	1.508	9.048	9.98
19	709	0.16–0.1	2.5–2.75	5	–	0	1.503	9.018	9.96
20	67/2G	0.4–0.2	2.55–2.61	11	1	3	1.503	9.018	9.98
21	Kul1	0.315–0.2	2.7–2.75	5	–	0	1.510	9.060	9.96
22	Kul2	0.2–0.16	2.6–2.7	–	–	–	1.509	9.054	–
23	Kul2	0.315–0.2	2.7–2.75	–	–	–	1.509	9.054	–
24	Bsh10	0.25–0.16	2.7–2.8	4	–	0	1.510	9.060	9.96
25	Bsh11	0.25–0.16	2.6–2.7	6	–	0	1.508	9.048	9.95
26	Bsh12	0.25–0.2	2.7–2.75	6	–	0	1.510	9.060	9.96
27	Bsh13	0.4–0.315	2.65–2.7	–	–	–	1.510	9.060	–
28	8à	0.1–0.063	2.7–2.75	8	2	3	1.507	9.042	9.98
29	60	0.315–0.2	2.6–2.7	10		0	1.507	9.042	9.94
30	60/3	0.16–0.1	2.65–2.7	5		0	1.505	9.030	9.94
31	24	0.1–0.063	2.6–2.7	8	2	3	1.505	9.030	–
32	903/6	0.5–0.2	2.5–2.65	–	–	–	1.506	9.024	–
33	43/4	0.63–0.315	2.6–2.65	8	3	2	1.508	9.048	9.98
34	314D	0.315–0.2	2.55–2.65	11	2	0	1.510	9.060	9.99
35	40/7	0.315–0.2	2.6–2.7	10	3	3	1.509	9.054	9.99
36	128	0.315–0.2	2.6–2.7	10	3	3	1.508	9.048	9.99
37	223I	0.16–0.1	2.65–2.75	8	2	3	1.507	9.049	9.99
38	70/23	0.4–0.2	2.7–2.8	–	–	–	1.508	9.048	–
39	70/19	0.4–0.2	2.65–2.75	5	–	0	1.509	9.054	9.96
40	85/5	0.4–0.315	2.75–2.8	6	2	0	1.511	9.066	9.97

Thickness of expandable smectite layers: Sm 16.85 Å, Verm 12.9–13.2 Å. Dash means the data are absent.

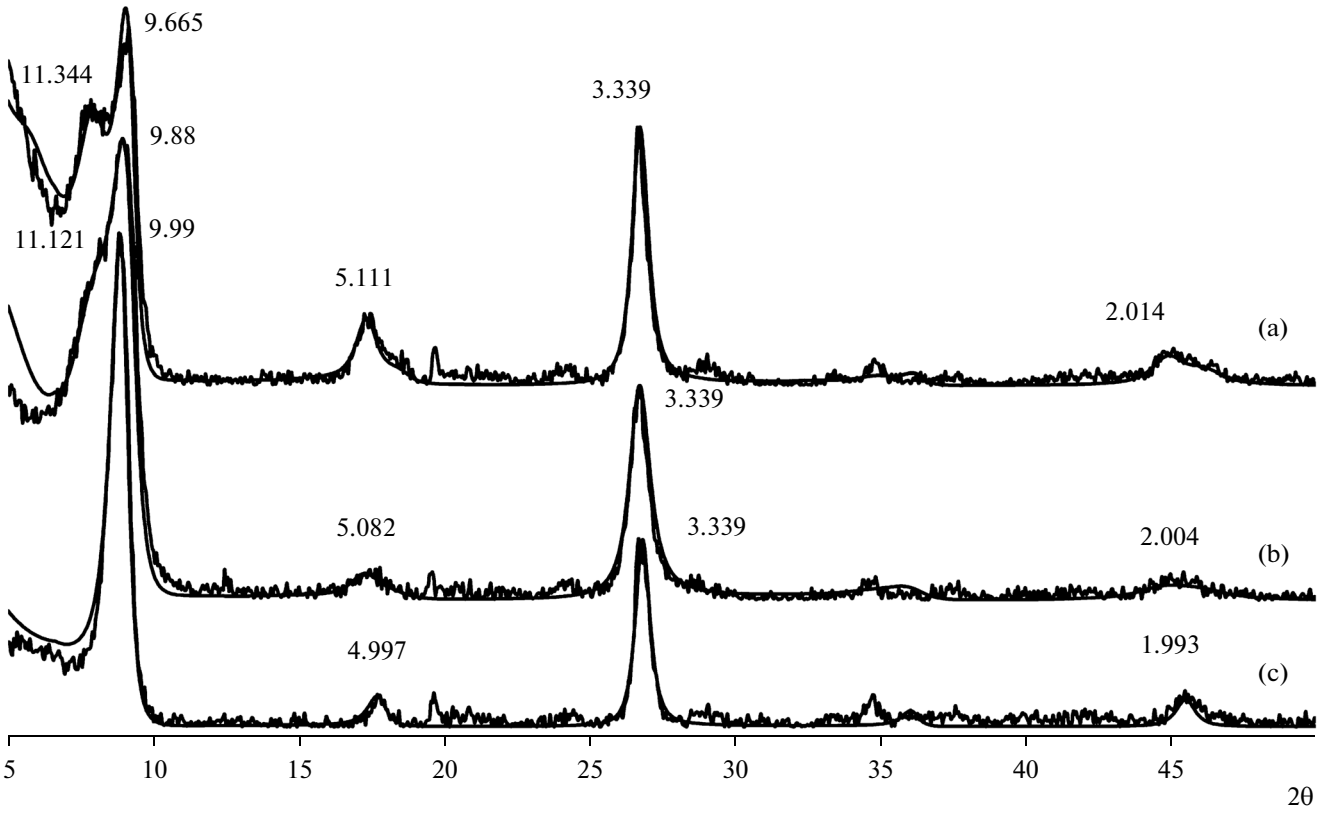

Fig. 7. Comparison of experimental and calculated powder diffraction patterns of glycolated oriented specimens. (a) Sample 67/2G, (b) sample 89, (c) sample BSh10. Straight and curved lines are calculated and experimental diffraction patterns, respectively.

No precision study has been performed for other samples of the studied collection. Judging from their diffraction patterns, where reflections with indices $\bar{1}12$ and 112 and indices $\bar{1}11$ and 021 slightly differ in the intensity and degree of resolution, they can be divided into the above three groups with different degrees of 3D ordering (Fig. 8). The high degree of structural ordering was noted for samples from the Lower Cambrian Pestrotsvet Formation (samples 544, 543, 541, 99/9) (Fig. 8a) and the Middle Riphean Totta Formation (sample 70/19). The middle degree of structural ordering is typical of samples 128, 85/5 and 96/2 (Middle Riphean Totta Formation and Rovno Horizon of the Podolian area). In particular, the diffraction pattern of sample 128 shows less intense reflections with d = 3.663 and 3.077 Å, lower intensity of reflections with d = 4.357 Å, and a broad low-intensity reflection with d ~ 4.13 (Fig. 8b). The structure of samples 40/7 and 43/4 (Middle Riphean Totta Formation) is characterized by the low degree of 3D ordering (Fig. 8c) similar to that of sample 314D.

The diffraction patterns of random specimens of most studied samples contain one reflection within the 060 region (d(060) = 1.503–1.518Å); parameter *b* in the studied layer silicates varies from 9.018 to 9.108 Å, respectively (Table 2, an. 6–40). Such values of this parameter are typical of dioctahedral layer silicates of the glauconite–illite composition. In glauconites from the Lower Cambrian sequences of East Siberia (Aldan River) (samples 515, 544, 543, 541, 99/9), this region contains two reflections: one strong reflection with d = 1.512–1.517 Å (*b* = 9.072–9.102 Å) corresponds to Fe^{3+} mica (glauconite), while the second weak reflection with d = 1.497–1.501 Å (*b* = 8.98–9.01 Å) corresponds to Al-mica (Table 2, an. 1–5; Fig. 8a).

Thus, the studied layer silicates of the glauconite–illite series contain varieties with different contents of expandable layers: low (4–8%) and high (10–13%). The mixed-layer structure of different mineral varieties can be either two-component (mica–smectite) or three-component (mica–smectite–vermiculite), while the degree of short-range order in the alternation of different types of layers may vary (short-range factor R = 0, 2, and 3). The samples are subdivided into three groups with the high, middle, and low degree of 3D ordering. The third group includes only three samples of Al-glauconites from the Middle Riphean Totta Formation (Aim River) (samples 314D, 43/4, 40/7) (Fig. 8c). Parameter *b* (9.018–9.108 Å) of the studied samples is typical of dioctahedral layer silicates of the glauconite–illite composition. Two-phase

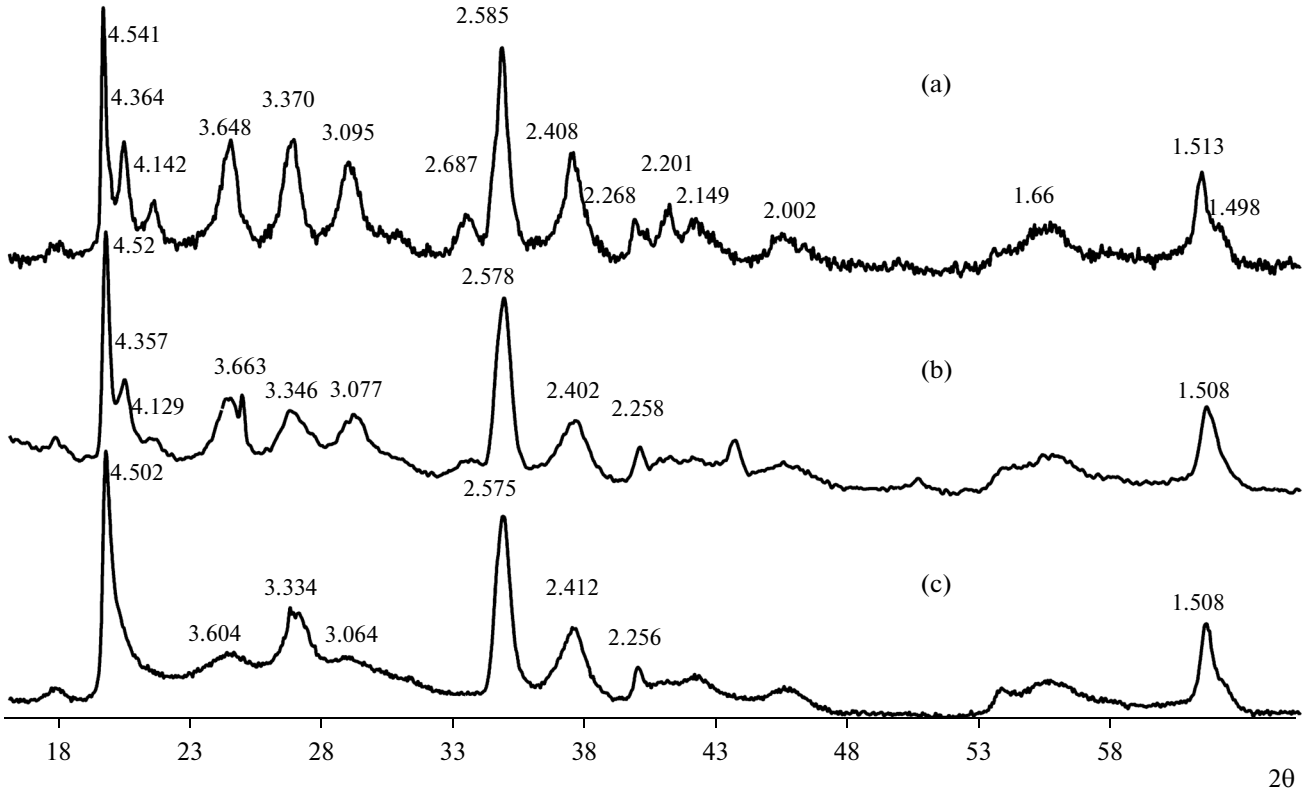

Fig. 8. Diffraction patterns of unoriented specimens. (a) Sample 541, (b) sample 128, (c) sample 43/4.

globules were found at the base of the Lower Cambrian Pestrotsvet Formation, East Siberia. Their random powder XRD patterns contain two reflections in the 060 region (Fig. 8a).

Electron Diffraction Data

Calculations of unit cell parameters and detailed electron diffraction studies with analysis of the degree of 3D ordering of samples were carried out by S.I. Tsipursky for the Lower Cambrian and Upper Proterozoic samples of East Siberia and Upper Riphean rocks of the South Urals (Tables 3, 4) (Ivanovskaya et al., 1989; Tsipursky et al., 1992). In addition, previously unpublished electron diffraction data are reported for sample 96/2 from the Vendian–Cambrian boundary rocks of the Podolian Dniester region (Table 3, an. 1).

In general, these studies confirmed the X-ray data and showed that the studied minerals are characterized by different degrees of structural ordering. Some samples are characterized by high-quality electron diffraction patterns (samples 515, 541, 543, 544, 99/9, 709, 558, 563, 70/23, 70/19, 85/5), while others show weak diffuse background and (or) weak "diffuse" reflections 02*l*, 11*l* (samples 67/2G, 8a, 60, 60/3, 24, 128, 223I). In three samples, these reflections become more "diffuse" up to their merging with the modulated background, indicating the high structural disorder (samples 43/4, 40/7, 314/D) (Ivanovskaya et al., 1989).

In addition, the electron diffraction studies confirmed the XRD data that globules from the Lower Cambrian Pestrotsvet Formation (samples 515, 544, 541, 99/9) contain two micaceous phases, which differ in the Fe index (Table 4) (Tsipursky et al., 1992). In sample 544, the two-phase composition of globules is determined only by the XRD method, while the OTED method indicates only one Fe-phase (glauconite) (Table 2, an. 2; Table 4). This results from of the higher accuracy of the XRD method as compared to the electron diffraction, which provides the analysis of only a limited number of microparticles. This reason also explains disagreement between *b* values calculated for the same samples by these two techniques (Tables 2–4).

Variations of Unit Cell Parameters b and csin β

Depending on the cation composition, the studied samples show significant variations of unit cell parameters *b* and csinβ. Illites have b = 9.02–9.05 Å and csinβ = 9.94–9.98 Å; Fe-illites and Al-glauconites are characterized by b = 9.02–9.08 Å and csinβ = 9.95–9.99 Å; and glauconites show b = 9.07–9.11 Å and csin csinβ = 9.985–10.0 Å. Parameter *b* tends to increase with increase of the content of octahedral Mg and Fe^{2+}

Table 3. Unit cell parameters of the studied samples on the basis of electron diffraction data

Analysis no.	Grain size, mm	Density, g/cm^3	Å			β, degree
			a	*b*	*c*	
96/2	0.315–0.2	2.6–2.65	5.23	9.05	10.24	101.1
709	0.16–0.1	2.5–2.75	5.21	9.02	10.17	101.2
67/2G	0.4–0.2	2.55–2.61	5.20	9.01	10.26	101.6
563	0.1–0.063	–	5.21	9.01	10.30	101.2
562	0.1–0.063	2.45–2.7	5.21	9.01	10.25	101.1
561	0.1–0.063	–	5.21	9.01	10.25	101.2
560	0.1–0.063	–	5.21	9.02	10.25	101.3
558I	0.1–0.063	–	5.21	9.01	10.30	101.2
8à	0.1–0.063	2.7–2.75	5.22	9.04	10.26	101.2
60	0.315–0.2	2.6–2.7	5.22	9.04	10.16	101.27
60/3	0.16–0.1	2.65–2.7	5.22	9.03	10.13	101.2
24	0.1–0.063	2.6–2.7	5.22	9.04	10.23	101.2
43/4	0.63–0.315	2.6–2.65	5.24	9.05	10.14	101.0
314D	0.315–0.2	2.55–2.65	5.23	9.05	10.18	~101
40/7	0.315–0.2	2.6–2.7	5.23	9.05	10.15	~101
128	0.315–0.2	2.6–2.7	5.23	9.05	10.21	101.2
223I	0.16–0.1	2.65–2.75	5.21	9.03	10.18	101.2
70/23	0.4–0.2	2.7–2.8	5.23	9.05	10.00	101.3
70/19	0.4–0.2	2.65–2.75	5.23	9.06	10.06	100.7
85/5	0.4–0.315	2.75–2.8	5.23	9.06	10.17	101.0

Dash means the data are absent.

Table 4. Electron diffraction data on glauconite and illite in the globules from the Lower Cambrian rocks (East Siberia)

Analysis no.	Grain size, mm	Density, g/cm^3	Unit cell parameters				
			glauconite				illite
			a, Å	*b*, Å	*c*, Å	β, degree	*b*, Å
515	0.16–0.1	2.75–2.8	5.24	9.08	10.15	101.0	9.00
544	0.1–0.063	2.75–2.8	5.23	9.07	10.15	101.0	–
541	0.4–0.2	2.7–2.8	5.26	9.06	10.14	101.1	9.00
99/9	0.4–0.2	2.65–2.75	5.26	9.09	10.18	101.2	9.00

Dash means the data are absent.

cations and decrease of $^{VI}Al/(^{VI}Al + {}^{VI}Fe^{3+})$ (Tables 1, 2; Fig. 9).

The wide scatter of data in Fig. 9 indicates a complicated dependence of parameter *b* of dioctahedral layer silicates on their composition. In general, similar tendencies were noted in (Zviagina and Drits, 2015), who demonstrated that increase of the contents of Si and Mg cations in the illite–aluminoceladonite series of the high-Al dioctahedral micas is accompanied by increase of parameter *b* and its subsequent decrease starting from the Si and Mg contents of ≥3.7 and 0.6 f.u., respectively. It is shown in (Drits et al., 2010; Zviagina and Drits, 2015) that csinβ in the dioctahedral 1M micas is mainly determined by the degree of Al for Si substitution in tetrahedra. In particular, the increase of csinβ in Al-rich micas of the illite–aluminoceladonite series with the increase of tetrahedral Al cations is described by the second-order function. In the studied samples, this dependence is not so clear, possibly suggesting that if $(Fe^{2+}+Fe^{3+}) > 0.3$ f.u., the csinβ value is determined by the cation composition of not only tetrahedral but also octahedral sheets. The detailed anal-

ysis of the dependence of unit cell parameters of high-Fe 2 : 1 dioctahedral layer silicates is a subject for a separate study.

IR Spectra of Micaceous Minerals of the Glauconite–Illite Series

The IR spectra of glauconite (sample 541), Fe-illite (samples Bsh11, Kul2), and illites (samples 70/19, 60) in a range of 400–1300 cm^{-1} and 3200–3800 cm^{-1} are shown in Fig. 10. The position and profile of the absorption bands in the IR spectra are typical of the dioctahedral micaceous minerals and correspond to the peculiarities of the cation composition of the studied samples.

The most intense IR bands are observed in the region of bending and stretching Si–O vibrations (triplet at 410–540 cm^{-1} and intense maximum at 1072–1087 cm^{-1}, respectively). Of special importance for diagnostic purposes is the OH stretching region (3200–3800 cm^{-1}).

Si–O bending and stretching vibrations. Increase in the content of Fe cations from illites to glauconites is accompanied by decrease of the resolution of bending Si–O bands and shift of two outer bands in triplet (427–437 cm^{-1} and 522–484 cm^{-1}) toward the middle band (471–459 cm^{-1}). Both bands in the Si–O stretching region are shifted toward lower wave numbers (from 1006 to ~ 1000 cm^{-1} and from 1085–1087 to 1072 cm^{-1}) (Fig. 10a).

OH stretching vibrations. Spectra of all studied samples, except sample 60, contain , in addition to a broad band at 3200–3400 cm^{-1} assigned to the absorbed water vibrations (Fig. 10b), two broad intense bands: one with the maximum at 3531–3536 cm^{-1} and another at 3603–3607 cm^{-1} (samples 70/19, Bsh11, Kul2) and 3621 cm^{-1} (sample 541). These bands result from a superposition of individual cation–OH–cation absorption bands. The first band corresponds to FeOHFe and FeOHMg vibrations; the second, to AlOHMg and AlOHAl vibrations. It should be noted that the assignment of individual absorption bands to specific cation pairs linked through an OH group was carried out according to the interpretation (Besson and Drits, 1997).

The most intense band in the glauconite spectrum (sample 541) is the band corresponding to FeOHFe vibrations with maximum at 3535 cm^{-1} corresponding to $Fe^{3+}OHFe^{3+}$ vibration and a shoulder at 3561 cm^{-1} ($Fe^{3+}OHMg$ and (or) $AlOHFe^{2+}$). The second well-resolved band results from the superposition of bands 3606 (AlOHMg) and 3623 cm^{-1} (Fig. 10b). Taking into account the comparatively low content of octahedral Al cations in the sample, the latter band may refer to AlOHAl vibrations of mica and $Fe^{3+}OHFe^{3+}$ vibrations in pyrophyllite structural fragments, which is also consistent with the presence of AlOHAl band (pyrophillite) at 3674 cm^{-1} (Besson and Drits, 1997).

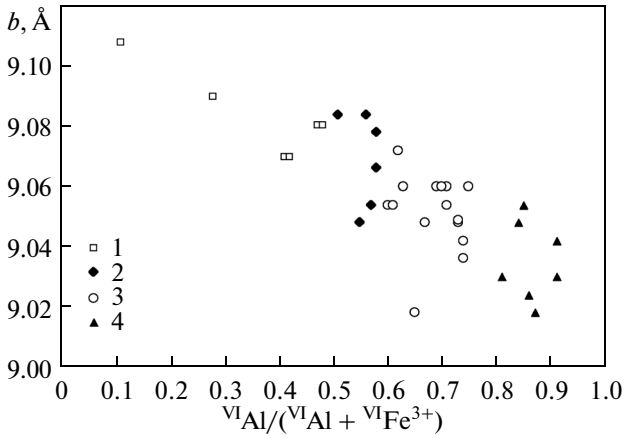

Fig. 9. Correlation between unit cell parameter *b* and $^{VI}Al/(^{VI}Al+ {}^{VI}Fe^{3+})$ for the studied layer silicates. (1) Glauconite, (2) Al-glauconite, (3) Fe-illite, (4) illite.

Samples of Fe-illites (samples Kul2, Bsh11) from two sections of the lower subformation of the Uk Formation, South Urals (Figs. 1b, 2b) are similar in composition (Table 1, an. 43, 45). However, their spectra differ dramatically in profile in the OH stretching region (Figs. 10b, 11). Sample Kul2 shows 3603 and 3533 cm^{-1} bands with close intensity, whereas the band at 3605 cm^{-1} in sample Bsh11 is much more intense. It was shown by (Dainyak et al., 2009) that these features are related to different patterns in the local distribution of cations in the structure of these samples. Figure 11 demonstrates the results of decomposition and fitting of spectra of samples Bsh11 and Kul2 (Dainyak et al., 2009). The spectra of the two samples differ both in sets and in relative contributions of individual components. These peculiarities may be associated with the specifics of microcrystal growth under non-equilibrium physicochemical conditions of the reduction zone in different parts of the shallow-water lower Uk basin.

Two regions are also distinguished in the illite spectrum (sample 70/19): the most intense band at 3607 cm^{-1} (superposition of AlOHMg and AlOHAl bands) and less intense band with maximum at 3531 cm^{-1} (FeOHFe). In addition, there is also a band at 3558 cm^{-1} ($Fe^{3+}OHMg$). Illite (sample 60) displays one broad band at 3605 cm^{-1} resulting from the superposition of individual cation–OH–cation absorption bands with the AlOHMg vibrations prevailing. It is noteworthy that the spectrum of illite 70/19 is more similar in shape to that of Fe-illite Bsh11 than to the spectrum of illite 60 (Fig. 10b). This may imply that the distinction between illites and Fe-illites in mica classification should take into account not only the contents of Al and Fe^{3+} cations but also the contents of Fe^{2+}.

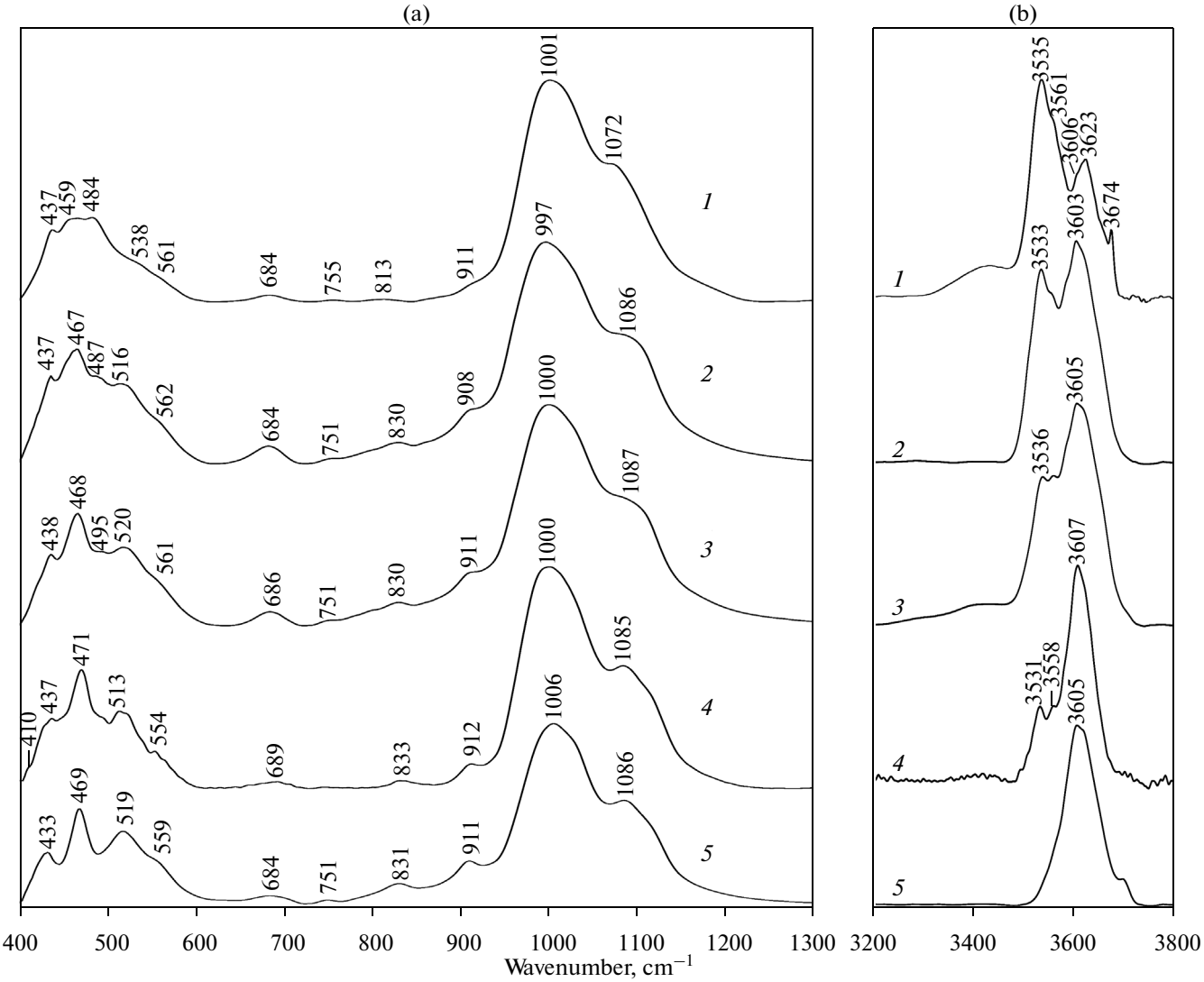

Fig. 10. IR spectra of samples of the illite–glauconite series in the region:(a) 400–1400 cm^{-1}, (b) 3200–3800 cm^{-1}. (*1*) Sample 541, (*2*) sample Kul2, (*3*) sample Bsh11, (*4*) sample 70/19, (*5*) sample 60.

Peculiarities of Mg-rich Mineral Varieties

While analyzing the structural and crystal-chemical features of the studied samples, let us examine in detail the globular layer silicates of the glauconite–illite composition with high contents of Mg cations (0.40–0.75 f.u.) taken from different lithologies.

Illites and Fe-illites. The highest content of Mg cations (0.65–0.75 f.u.) in the studied collection was found in three samples ascribed to Fe-illite (sample 709) and illite proper (samples 70/23, 70/19) (K_{Al} = 0.65 and 0.84, 0.85, respectively). The sum of octahedral cations in their structural formula varies from 2.14 to 2.17 at the unit cell anion composition of $O_{10}(OH)_2$ (Table 1, an. 39, 63, 64). Note that the first sample is confined to dolomites of the Vendian Yudoma Formation, while two others were taken from thin sandstone units intercalated in the section with dolomites and mudstones (Middle Riphean, Totta Formation, MH) (Fig. 3c) (Ivanovskaya et al., 1985, figure).

The detailed structural and crystal–chemical study of Al-glauconite (K_{Al} = 0.57) with high Mg content (0.63 f.u.) from dolomites of the Yusmastakh Formation (Riphean, Anabar Rise) (sample 501) revealed the micaceous (90%), smectite (6%), and di-trioctahedral chlorite (4%) layers. The high Mg index of the minerals is related both to the presence of Mg-bearing brucite-type interlayers in the di-trioctahedral chlorite and to the high Mg content in the octahedral sheets of 2 : 1 layers. These features are related to the formation of glauconite in dolomite sediments under disequilibrium conditions of the reduction zone in a shallow-water basin with a sufficiently high content of Mg cation (Drits et al., 2010).

Unlike sample 501, the simulation of mineral varieties with the high Mg content revealed no chlorite

layers, and only smectite layers of variable thickness (16.85 Å and 12.9–13.2 A) were recorded (Table 2, an. 1, 2, 4, 19, 24–26, 29, 39, 40). Note that the ~ 12.9–13.2 Å layers are ascribed to the vermiculite-type or high-charge expandable smectite layers.

The above-described mineral varieties (samples 709, 70/19) have the following properties: expandable layers 5%; $b = 9.02, 9.05$ Å; and $c\sin\beta = 9.96$ Å (Table 2, an. 19, 39). The presence of interlayer Mg cations in samples 709 and 70/23 (~0.03–0.04 f.u.) was experimentally shown by Tsipursky (Ivanovskaya et al., 1989). In terms of the cation composition, samples 70/19 and 70/23 are close to aluminoceladonites (contents of Si and Mg cations are ~3.7 and 0.7 f.u., respectively) (Table 1, an. 63, 64). However, the values of b and $c\sin\beta$ (Table 2, an. 38, 39) significantly exceed those typical of aluminoceladonites (Zviagina and Drits, 2015), while the sum of octahedral cations is ≥2.15. Therefore, additional high-precision X-ray studies are required to determine the crystal-chemical nature of these Mg-rich samples.

The high Mg content in Fe-illite (sample 709) can be related to the conditions of globule formation in the dolomite sediment, while illite globules (samples 70/23, 70/19) in the Totta Formation (MH, East Siberia) were formed mainly in thin sand strata among clay interbeds (Fig. 3c) intercalated with dolomite. In this case, the grains of layer silicates were formed in the sandy-clayey sediments owing to intense reduction, which follows from the high contents of Fe^{2+} (0.27, 0.29 f.u.) in the mineral structure (Table 1, an. 63, 64) and the presence of large organic-walled microfossils described by A.F. Veis in the mudstones and clay siltstones of this section, in particular, in sample 70/19 (Ivanovskaya et al., 1984). According to (Nikolaeva, 1977), intensification of reduction is accompanied by increase of the degree of saturation of mud waters in both Fe^{2+} cations and Mg.

Two illite samples from mudstones (sample 60) and clayey siltstones (sample 60/3) of the Inzer (?) Formation of the South Urals are characterized by the lowest contents of Fe^{3+} and Fe^{2+} cations (0.13 and 0.15, 0.16 f.u.) with high contents of Mg cations (Mg = 0.45, 0.40 f.u.) and high Al index ($K_{Al} = 0.91$) (Fig. 3d; Table 1, an. 54, 55). In these samples, the content of smectite layers varies from 5 to 10% (samples 60/3 and 60, respectively), $b = 9.03, 9.04$ Å, and $c\sin\beta = 9.94$ Å (Table 2, an. 29, 30). Organic matter (C_{org}) facilitating the formation of globular silicates is present as variably preserved filamentous microfossils found by N.G. Vorob'eva in sample 60. Three samples of Fe-illites (samples Bsh10, 12, 13) taken from the coarser sandy–silty rocks of the Uk Formation (Zilim River, South Urals) have sufficiently high contents of Mg cations (Mg = 0.47–0.52 f.u.) and Fe^{2+} (0.29–0.37 f.u.) (Table 1, an. 44, 46, 47). These micaceous minerals (samples Bsh10, 12) contain from 4 to 6% smectite layers at $b = 9.05, 9.06$ Å and $c\sin\beta = 9.95, 9.96$ Å (Table 2, an. 24, 26).

Glauconites and Al-glauconites. High contents of Mg cations (Mg = 0.47–0.50 f.u.) were also found in the glauconites ($K_{Al} = 0.41–0.49$) from limestones of the Lower Cambrian Pestrotsvet Formation (samples 515, 606, 544, 541), which overlie dolomites of the Vendian Yudoma Formation (Aldan River, East Siberia) (Figs. 1c, 2a; Table 1, an. 3–5, 11), and in the Al-glauconite ($K_{Al} = 0.58$) from sandstones (sample 85/5) alternating with dolomites in the sequence of the Lower Riphean Enna Formation (East Siberia) (Fig. 1c, 2a; Table 1, an. 65). In these samples, the content of smectite layers varies from 5 to 8%, $b = 9.07–9.08$ Å, and $c\sin\beta = 9.97–10.0$ Å (Table 2).

In general, the b value in Mg-rich illite and Fe-illite samples with is slightly higher, while $c\sin\beta$ is lower than in the corresponding varieties with the lower Mg content. In glauconites and Al-glauconites, this trend is less expressed due to the possible effect of the high content of Fe cations.

The high content of Mg cations in the studied globular layer silicates of the glauconite–illite series can be caused by the intensity of reduction processes in the early diagenesis zone during the accumulation of sediments of different compositions and by other factors.

Structural and Crystal-Chemical Heterogeneity of the Studied Samples

The heterogeneity of glauconite grains on the macro- and microlevels (in polished thin section, sample, density fraction, and single grain) is a well-known fact (Shutov et al., 1972, 1975; Murav'ev and Voronin, 1975; Nikolaeva, 1977, 1981; Duplay, 1988; Tsipursky et al., 1992; Drits and Kossovskaya, 1986; Drits et al., 1993, 2010; Ivanovskaya, 1994, 1996; Ivanovskaya et al., 1999, 2012; Drits et al., 2013; and others). The data mentioned above show that the studied samples are also marked by heterogeneity on the mineralogical, structural, and crystal-chemical levels. Let us consider in detail their heterogeneity on the micro- and macrolevels (in a single grain and in separate density fractions).

Electron microdiffraction and local energy-dispersive analysis revealed a sufficiently high degree of chemical heterogeneity of microparticles that compose grains in carbonate rocks of the Lower Cambrian Pestrotsvet Formation in East Siberia (Aldan River) (Ivanovskaya and Tsipursky, 1982; Tsipursky et al., 1992). In particular, the study of sample 99/9 showed that micaceous minerals from a single globule define an isomorphic series, with the statistic predominance of particles enriched in Fe and depleted in Al. The predominant phase of this sample is glauconite ($b = 9.08$ Å). The second widespread phase (~35%) is illite ($b = 8.98$ Å). The general crystal-chemical formula of sample 99/9 and formulas of individual micaceous phases, as well as parameters b, are listed in Tables 1 (an. 7–9), 2, and 4. Similar two-phase globules were also found in the Lower Cambrian rocks of northern Estonia and Lower

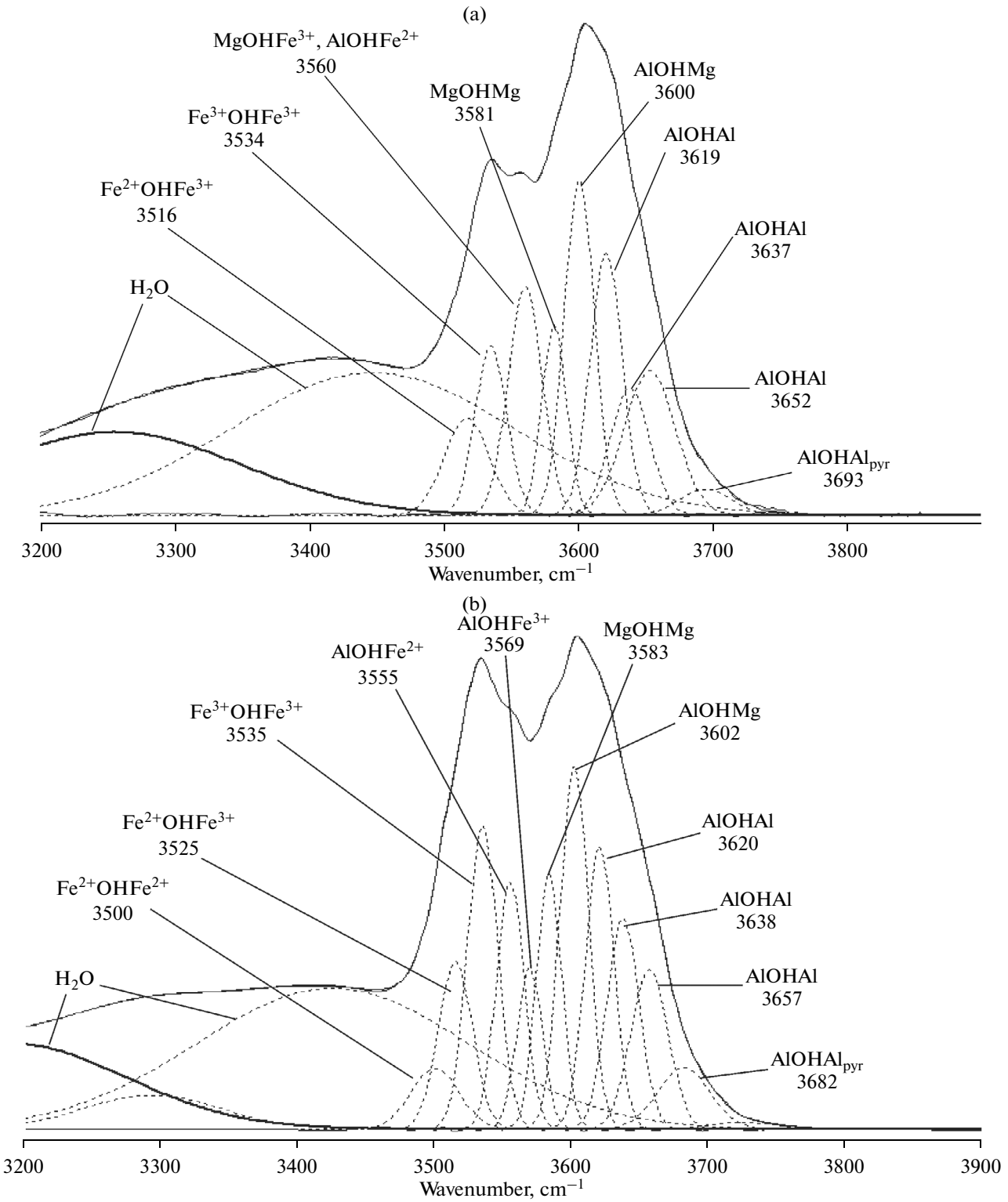

Fig. 11. Results of the decomposition and fitting of IR spectra of Fe-illites in the OH stretching region modified after (Dainyak et al., 2009). (a) Sample Bsh11, (b) sample Kul2.

Riphean rocks of North Siberia (Kotuikan River) (Tsipursky et al., 1992).

The microprobe studies of samples from the Vendian–Cambrian rocks of the Khmel'nistkaya Formation of the Podolian Dniester region carried out by researchers under the supervision of V. Drits discovered that the two-phase composition of micaceous minerals is manifested not only on the microlevel within individual globules, but also in different globules. In particular, the study of dark green globules in sample 94 (0.315–0.2 mm, 2.7–2.75 g/cm^3) revealed that they are homogenous in composition but substantially different in the Fe content and are represented by glauconites and Fe-illites amounting to 75 and 25%, respectively (Ivanovskaya et al., 1999). Their crystal-chemical formula and the average composition of globules are shown in Table 1 (an. 26–28). The compositional heterogeneity of the micaceous minerals on the macrolevel can be explained by their crystallization in sediments with uneven distribution of cation composition and redox potential in the mud waters. Similar conditions of mineral formation environment have also been noted on the microlevel during the crystallization of micaceous minerals with different Fe mole fractions in a single globule, as has been mentioned above for the two-phase globule and was documented by microprobe studies in other fractions of sample 94 (Tsipursky et al., 1992; Ivanovskaya et al., 1999).

In one of the recent works dedicated to microcrystal-chemical heterogeneities of the Precambrian globular dioctahedral 2 : 1 layer silicates (Drits et al., 2013), it was shown by the simulation of the powder diffraction patterns that each of the studied samples represents a physical mixture of individual micaceous phases with different cation compositions. In particular, the phase composition of globules from sample 60 (0.315–0.2 mm, density 2.6–2.7 g/cm^3) is represented mainly by illite (77%) and Fe-illite (17%).

CONCLUSIONS

The studied dioctahedral 2 : 1 layer silicates from the catagenetically transformed Upper Proterozoic and Lower Cambrian rocks are characterized by wide variations of the isomorphic substitution of octahedral Fe, Al, and Mg cations. Based on the IMA NC and AIPEA NC classification and the paper (Kossovskaya and Drits, 1971), they represent a continuous isomorphic series from glauconite via Al-glauconite and Fe-illite to illite (K_{Al} = 0.11–0.50, 0.51–0.58, 0.61–0.78, and 0.81–0.91, respectively).

In addition to the cation composition, b and $c\sin\beta$ values and characteristics of IR spectra can serve as diagnostic criteria for the identification of individual varieties of micaceous minerals of the glauconite–illite series. The results of IR spectroscopic studies showed that not only the proportions of Al and Fe^{3+} cations, but also the content of Fe^{2+} cations should be taken into account in the distinction between illites and Fe-illites.

Based on the previously obtained (Ivanovskaya et al., 2012) and new data, variations of the cation composition in the studied mineral varieties fall beyond the fields proposed by IMA NC and approved by AIPEA NC. Therefore a revision of the existing classification of low-charge dioctahedral micaceous minerals may be required.

ACKNOWLEDGMENTS

This work was supported by the Russian Foundation for Basic Research (project nos. 13-05-00127, 14-05-00323, and 15-05-09095) and by the Presidium of the Russian Academy of Sciences (Priority program no. 29).

We are grateful to Prof. V.A. Drits for consultations during the manuscript preparation and N.G. Vorob'eva for the microphytological analysis of samples.

REFERENCES

Bailey S.W., Brindley G.W., Kodama H., Martin R.T. Report of the Clay Minerals Society Nomenclature Committee for 1977 and 1978, *Clays Clay Miner.,* 1979, vol. 27, no. 3, pp. 238–239.

Bailey, S.W., Brindley, G.W., Fanning, D.S., et al., Report of the Clay Minerals Society Nomenclature Committee for 1982 and 1983, *Clays Clay Miner.*, 1984, vol. 32, no. 3.

Bekker, Yu.R., Negrutsa, V.Z., and Polevaya, N.I., Age of glauconite horizons and upper boundary of Hyperborean in the eastern Baltic Shield, *Dokl. Akad. Nauk*, 1970, vol. 193, no. 5, pp. 1123–1126.

Besson, G. and Drits, V.A., Refined relationships between chemical composition of dioctahedral fine-dispersed mica minerals and their infrared spectra in the OH stretching region. Part I. Identification of the stretching bands, *Clays Clay Miner.*, 1997, vol. 45, pp. 158–169.

Dainyak, L.G., Rusakov, V.S., Ivan, A., Sukhorukov, V.S., et al., An improved model for the interpretation of Mössbauer spectra of dioctahedral 2 : 1 *trans*-vacant Fe-rich micas: refinement of parameters, *Eur. J. Miner.*, 2009, vol. 21, pp. 995–1008.

Drits, V.A. and Kossovskaya, A.G., Genetic types of dioctahdedral micas: Communication 1. Family of Fe–Mg silicates (glauconites, celadonites), *Litol. Polezn. Iskop.*, 1986, no. 5, pp. 19–34.

Drits, V.A. and Kossovskaya, A.G., Clay minerals: Micas and chlorites, *Tr. GIN AN SSSR*,, 1991, no. 465.

Drits, V.A. and Sakharov, B.A., *Rentgenostrukturnyi analiz smeshanosloinykh mineralov* (The X-Ray Structural Analysis of Mixed-Layer Minerals), Moscow: Nauka, 1976.

Drits, V.A., Kameneva, M.Yu., Sakharov, B.A., et al., *Problemy opredeleniya real'noi struktury glaukonitov i rodstvennykh tonkozernistykh fillosilikatov* (Problems in Identification of the Real Structure of Glauconites and Cognate Fine-Grained Phyllosilicates), Novosibirsk: Nauka, 1993.

Drits, V.A., Zviagina, B.B., McCarty, D.K., and Salyn, L.A., Factors responsible for crystal-chemical variations in solid

solutions from illite to aluminoceladonite and from glauconite to celadonite, *Am. Miner.*, 2010, vol. 95, pp. 348–361.

Drits, V.A., Ivanovskaya, T.A., Sakharov, B.A., et al., Nature of the structural and crystal-chemical heterogeneity of the Mg-Rich glauconite (Riphean, Anabar Uplift), *Lithol. Miner. Resour.*, 2010, no. 6, pp. 555–576.

Drits, V.A., Sakharov, B.A., Ivanovskaya, T.A., and Pokrovskaya, E.V., Crystal-chemical microheterogeneity of Precambrian globular dioctahedral mica minerals, *Lithol. Miner. Resour.*, 2013, no. 6, pp. 489–515.

Duplay, J., Geochemie des argiles et geothermometrie des populations monominerales de particules, *These pour obtenir le grade de docteur le sciences*, Strasburg: Instit. Geol., 1988.

Ericsson, T. and Wappling, R., Texture effects in 3/2-1/2 Mössbauer spectra, *J. Phys. Colloques*, 1976, vol. 37, no. C6, pp. 719–723.

Geptner, A.R. and Ivanovskaya, T.A., Glauconite from Lower Cretaceous marine terrigenous Rocks of England: A concept of biochemogenic origin, *Lithol. Miner. Resour.*, 2000, no. 5, pp. 434–444.

Gorokhov, I.M., Yakovleva, O.V., Semikhatov, M.A., and Ivanovskaya, T.A., The Rb–Sr and K–Ar age and Mössbauer spectra of globular layer silicates of the glauconite series: The Middle Riphean Debengda Formation in the Olenek Uplift, North Siberia, *Litol. Polezn. Iskop.*, 1995, no. 6, pp. 615–631.

Gorokhov, I.M., Yakovleva, O.V., Semikhatov, M.A., et al., Rejuvenated" Al-glauconite in Vendian–Cambrian deposits of the Podolian Dniester region, Ukraine: Rb–Sr and K–Ar systematics and ^{57}Fe Mössbauer spectra, *Lithol. Miner. Resour.*, 1997, no. 6, pp. 541–558.

Guggenheim, S., Adams, J.M., Bain, D.C., et al., Summary of recommendations of Nomenclature Committees relevant to clay mineralogy: report of the Association Internationale pour l'etude des Argiles (AIPEA) Nomenclature Committee for 2006, *Clays Clay Miner.*, 2006, vol. 54, pp. 761–772.

Ivanovskaya, T.A., Glauconite–illite minerals in the Upper Vendian–Lower Cambrian boundary deposits of the Podol'sk Dniester region, *Lithol. Miner. Resour.*, 1996, no. 6, pp. 524–534.

Ivanovskaya, T.A., Glauconitites in terrigenous rocks of the Khaipakh Formation (Middle Riphean, Olenek Uplift), *Lithol. Miner. Resour.,* 2009, no. 4, pp. 348–366.

Ivanovskaya, T.A. and Tsipurskii, S.I., Peculiarities of glauconite from the Lower Cambrian rocks in the Ulakhan-Sulugur section, *Litol. Polezn. Iskop.*, 1982, no. 4, pp. 78–86.

Ivanovskaya, T.A. and Zaitseva, T.S., Dioctahedral 2 : 1 phyllosilicates of the illite–glauconite series of the Precambrian and Lower Cambrian deposits, *Acta Miner.-Petrogr. Abstract Ser.,* 2015, vol. 9.

Ivanovskaya, T.A., Tsipurskii, S.I., Cherkashin, V.I., and Yakhontova, L.K., Postsedimentary transformations of glauconite from Riphean rocks in southeastern Yakutia, *Izv. Akad. Nauk SSSR, Ser. Geol.*, 1985, no. 12, pp. 108–118.

Ivanovskaya, T.A., Tsipurskii, S.I., and Yakovleva, O.V., Mineralogy of Riphean and Vendian globular layer silicates in Siberia and the Urals, *Litol. Polezn. Iskop.,* 1989, no. 3, pp. 83–99.

Ivanovskaya, T.A., Sakharov, B.A., Gor'kova, N.V., et al., Berthierine in catagenetically altered Vendian–Cambrian deposits of Podolia, Dniester region, *Lithol. Miner. Resour.*, 1999, no. 2, pp. 170–183

Ivanovskaya, T.A., Zaitseva, T.S., Gorokhov, I.M., and Konstantinova, G.V., Mineralogical, Mössbauer, and isotopic–geochronological study of Upper Riphean Al-glauconites, Kil'din Group, Srednii Peninsula, *Lithol. Miner. Resour.*, 2003, no. 5, pp. 447–456.

Ivanovskaya, T.A., Zaitseva, T.S., Zvyagina, B.B., and Sakharov, B.B., Crystal-chemical peculiarities of globular layer silicates of the glauconite–illite composition (Upper Proterozoic, northern Siberia), *Lithol. Miner. Resour.*, 2012, no. 6, pp. 491–513.

Ivanovskaya, T.A., Zaitseva, T.S., and Zviagina, B.B., *Crystal-chemical peculiarities of globular layer silicates of the illite–glauconite series in the Upper Proterozoic and Vendian–Cambrian deposits (Siberia, Southern Urals, Srednii Peninsula, Russia and Podolia, Ukraine)*, 2nd Int. Conf.: Clays, Clay Minerals and Layered Minerals (CMLM), St. Petersburg: Falcon print, 2013.

Karlova, G.A. and Vodanyuk, S.A., New data on the transitional to Cambrian rocks in the Khorbusuonka River basin (Olenek Uplift), in *Stratigrafiya pozdnego dokembriya i rannego paleozoya Sibiri. Vend i rifei* (Stratigraphy of Late Precambrian and Early Paleozoic in Siberia: Vendian and Riphean), Novosibirsk: Nauka, 1985, pp. 3–13.

Kossovskaya, A.G. and Drits, V.A., Issues of the crystal-chemical and genetic classification of micaceous minerals in sedimentary rocks, in *Epigenez i ego mineral'nye indikatory* (Epigenesis and Its Mineral Indicators), Moscow: Nauka, 1971.

Missarzhevskii, V.V., The Cambrian–Precambrian boundary layers on the western slope of the Olenek Uplift (Olenek River), *Byull. Mosk. O-va Ispyt. Prir., Otd. Geol.*, 1980, vol. 85, pp. 23–34.

Murav'ev, V.I. and Voronin, B.I., Heterogeneity of the composition of glauconite grains, *Litol. Polezn. Iskop.*, 1975, no. 3, pp. 74–84.

Nikolaeva, I.V., *Mineraly gruppy glaukonita v osadochnykh formatsiyakh* (Minerals of the Glauconite Group in Sedimentary Formations), Novosibirsk: Nauka, 1977.

Nikolaeva, I.V., Facies zonation of the chemical composition of glauconite group minerals and its governing factors, in *Mineralogiya i geokhimiya glaukonita* (Mineralogy and Geochemistry of Glauconite), Novosibirsk: Nauka, 1981, pp. 4–41.

Odin, G.S., Application de la microscopie electronique par réflexion à l'étude des minéraux argileux: exemple des minéraux des glauconites, *Trav. Labor. Micropaleont.,* 1974, no. 3, pp. 297–313.

Pfannes, H.D. and Gonser, U., Goldanskii-Karyagin effect versus preferred orientation (texture), *Appl. Phys.*, 1973, vol. 1, pp. 93–102.

Rieder, M., Cavazzini, G., D'yakonov, Y., et al., Nomenclature of the micas, *Can. Miner.*, 1998, vol. 36, pp. 41–48.

Sakharov, B.A. and Drits, V.A., Technique for determination of the content of smectite layers in the dispersed dioctahedral K-bearing micaceous minerals, *Lithol. Miner. resour.*, 2015, no. 1, pp. 50–79.

Sakharov, B.A., Besson, J., Drits, V.A., et al., Study of the nature of packing defects in the glauconite structure by the

diffraction profile analysis, *Izv. Akad. Nauk SSSR, Ser. Geol.*, 1990, no. 12, pp. 97–109.

Sakharov, B.A., Lindgreen, H., Salyn, A., and Drits, V.A., Determination of illite–smectite structures using multispecimen X-ray diffraction profile fitting, *Clays Clay Miner.*, 1999, vol. 47.

Semikhatov, M.A., The Upper Precambrian, in *Sostoyanie izuchennosti stratigrafii dokembriya i fanerozoya Rossii. Zadachi dal'neishikh issledovanii. Postanovleniya Mezhvedomstvennogo stratigraficheskogo komiteta i ego postoyannykh komissii* (State of Knowledge of the Precambrian and Phanerozoic Stratigraphy of Russia: Tasks for Further Studies), St. Petersburg: VSEGEI, 2008, iss. 38, pp. 15–27.

Semikhatov, M.A. and Serebryakov, S.N., *Sibirskii gipostratotip rifeya* (The Siberian Hypostratotype of the Riphean), Moscow: Nauka, 1983.

Semikhatov, M.A., Gorokhov, I.M., Ivanovskaya, T.A., et al., The K–Ar and Rb–Sr age of Riphean and Cambrian globular layer silicates in the Soviet Union: Materials for evaluation of the geochronometer, *Litol. Polezn. Iskop.*, 1987, no. 5, pp. 78–96.

Sergeev, V.N., *Okremnennye mikrofossilii dokembriya: priroda, klassifikatsiya i biostratigraficheskoe znachenie* (Silicified Precambrian Microfossils: Nature, Classification, and Biostratigraphic Significance), Moscow: GEOS, 2006.

Shutov, V.D., Katz, M.Ya., Drits, V.A., and Sokolova, A.L., Crystallochemical heterogeneity of glauconite as depending on the conditions of its formation and postsedimentary changes, *Proc. Int. Clay Conf.,* Madrid, 1972, pp. 269–279.

Shutov, V.D. and Kats, M.Ya., Drits. V.A., et al., Crystal chemistry of glauconite as indicator of facies conditions of its formation and postsedimentary alteration, in *Kristallokhimiya mineralov i geologicheskie problemy* (Crystal Chemistry of Minerals and Geological Issues), Moscow: Nauka, 1975, pp. 74–81.

Sokolov, B.S., The Vendian System in the General Stratigraphic Scale of Russia, in *Prilozhenie k sborniku statei konferentsii: "Obshchaya stratigraficheskaya shkala Rossii: sostoyanie i perspektivy obustroistva"* (Supplement to the Collection of Works of the Conference "General Stratigraphic Scale of Russia: State and Perspectives of Arrangement), Moscow: GIN RAN, 2013.

Stratotip rifeya. Stratigrafiya. Geokhronologiya (The Riphean Stratotype: Stratigraphy, Geochronology), Moscow: Nauka, 1983, p. 184.

Tsipurskii, S.I., Ivanovskaya.T.A. Crystal Chemistry of globular layer silicates, *Litol. Polezn. Iskop.*, 1988, no. 1, pp. 41–49.

Tsipurskii, S.I., Ivanovskaya.T.A., Sakharov B.A., et al., Nature of the coexistence of glauconite, Fe-illite, and illite in globular micaceous minerals in rocks of different lithological types and ages, *Litol. Polezn. Iskop.*, 1992, no. 5, pp. 65–75.

Veis, A.F., Kozlov, V.I., Sergeeva, I.D., and Vorob'eva, N.G., Microfossils from the Upper Riphean type section (the Karatau Group of Southern Urals), *Stratigr. Geol. Correlation*, 2003, vol. 11, no. 6, pp. 550–572.

Vend Podolii. Putevoditel' ekskursii II Mezhdunarodnogo simpoziuma po kembriiskoi sisteme i granitse venda i kembriya (The Vendian in Podolia: Guidebook for Excursions. 2nd International Symposium Devoted to the Cambrian System at the Vendian/Cambrian Boundary), Kiev: KGU, 1990.

Vodanyuk, S.A. and Karlova, G.A., The Kessyusa Formation in the Olenek Uplift, in *Pozdnii dokembrii i rannii paleozoi Sibiri. Rifei i vend* (Late Precambrian and Early Paleozoic of Siberia: Riphean and Vendian), Novosibirsk: Nauka, 1988, pp. 3–20.

Zaitseva, T.S., Gorokhov, I.M., Ivanovskaya, T.A., et al., Mössbauer characteristics, mineralogy and isotopic age (Rb–Sr, K–Ar) of Upper Riphean glauconites from the Uk Formation, the southern Urals, *Stratigr. Geol. Correlation*, 2008, vol. 14, no. 3, pp. 227–247.

Zviagina, B.B. and Drits, V.A., The illite-aluminoceladonite series: distiguishing features and identification criteria, *Acta Miner.-Petrogr. Abstract Ser.*, 2015, vol. 9.

Zviagina, B.B., McCarty, D.K., Srodon, J., and Drits, V.A., Interpretation of infrared spectra of dioctahedral smectites in the region of OH-stretching vibrations, *Clays Clay Miner.*, 2004, vol. 52, no. 4, pp. 399–410.